PAPER BASED LOW COST BIOSENSOR
DESIGN AND FABRICATION

by

Melike Nur Önder

Submitted to the Institute of Graduate Studies in

Science and Engineering in partial fulfillment of

the requirements for the degree of

Master of Science

in

Electrical and Electronics Engineering

Istanbul Bilgi University

2017

PAPER BASED LOW COST BIOSENSOR
DESIGN AND FABRICATION

APPROVED BY:

Assist. Prof. Dr. Y. Dağhan Gökdel   …………………………………….
(Advisor)

Assist. Prof. Dr. Özgür Gül   …………………………………….
(Co-advisor)

Prof. Dr. Sedat Ölçer   …………………………………….

Assist. Prof. Dr. Okan Zafer Batur   …………………………………….

Assist. Prof. Dr. Onur Ferhanoğlu   …………………………………….

DATE OF APPROVAL: …. /…./….

ACKNOWLEDGEMENT

I would like to mention about my gratitude to whom make this thesis possible to complete.

Firstly, I would like to give my sincere gratitude to my advisor Asst. Prof. Dr. Y. Dağhan Gökdel and my co-advisor Asst. Prof. Dr. Özgür Gül. Throughout of my thesis, I am motivated and encouraged with their patience and guiding. Their guiding is not only aspect of project, they also lead me to my career plans and encourage me to relief my best.

Being a member of Micro-System Lab and part of Biosensor Research Group make me feel lucky. I would like to thank all the members in both Micro-System Lab and Biosensor Research Group.

I am gratitude to have such team mates Ö. Gökalp Akcan and Tuğçe Ayraç. I am thankful for their help and motivation.

I would also thank to Prof. Dr. Ahmet Denker to encourage me to study at master degree and Prof. Dr. Sedat Ölçer for his comments and without his support, it would not be possible to complete this project.

Finally, I would like to express my appreciation to my family. I owe my parents Ayfer Önder and Murat Önder so much for their tolerance, understandings and supports. I am grateful my sister Gökçe Gül Önder, my friends Akın Kaya and Taylan Parlak for their continuous pertinacity to motivate me.

ABSTRACT

PAPER BASED LOW COST BIOSENSOR
DESIGN AND FABRICATION

MEMS devices as being one of the incrementally developing field with micro scale range and higher sensitivity are quite valuable. In the scope of this thesis, a paper-based MEMS device is produced with a low cost and fast fabrication procedure. The sensor, which is designed to measure weights, can be easily modified as a biosensor. Hence, the most important parameter of this sensor is its sensitivity.

The sensor measures the magnitude of the applied force by using the change in piezoresistor which is directly proportional to the applied force. Piezoresistive material coated sensor, which is designed as a cantilever shaped structure, is electrically connected to the Wheatstone bridge circuit. Graphite ink is used as a piezoresistor due to the ease of implementation. Paper-based sensor measures the weight by using the direct relation between the voltage change (Wheatstone bridge circuit output) and applied force excited on the cantilever.

The novelty of this sensor is addition of magnetic amplifier. The advantage of magnetic amplifier is to increase the effective mass of the weight. This addition provides 0.3 mg resolution measurement from 20 mg resolution weight sensor.

This sensor can only quantify the weights that are magnetically active. Furtherance, it can be easily transformed to a biosensor. The only thing that is necessary is to bind the MNP (magnetic nano particle) and the biological/chemical particle to make it a magnetically active component. After the binding process, these components can be detectable and measurable by this weight sensor that uses the magnetic mass increase scheme.

ÖZET

KAĞIT TABANLI DÜŞÜK MALİYETLİ BİYOALGILAYICI TASARIMI VE ÜRETİMİ

Hızla gelişen alanlardan biri olan MEMS cihazları mikro boyutlarda olmaları ve yüksek hassasiyete sahip olmaları dolayısıyla oldukça önem arz etmektedirler. Bu proje kapsamında ucuz ve hızlı üretim tekniklerine sahip olması sebebiyle son zamanlarda en çok ilgilenilen alanlardan biri olan kağıt tabanlı algılayıcı üretilmiştir. Bu proje kapsamında, ağırlık ölçümlerinde kullanılmak için üretilen bu algılayıcının biyoalgılayıcıya dönüştürülmesinin kolay olması istenmektedir. Bu nedenle de algılayıcının tasarım ve üretim aşamalarında en çok dikkat edilen kısım hassasiyetinin yüksek olmasıdır.

Yapılan algılayıcı piyezo malzemenin, uygulanan kuvvetle doğru orantılı değişen direncini ölçerek ağırlığın ölçümünü yapmaktadır. Piyezo malzeme uygulanmış dirsek şeklindeki algılayıcı, okuma devresi amacıyla, Wheatstone köprüsüne bağlanmıştır. Piyezo malzeme olarak üretim sürecini kolaylaştırması sebebiyle grafit esaslı macun kullanılmıştır. Wheatstone köprüsündeki voltaj değişimi grafit direncin değişimiyle, o da kağıda uygulanan kuvvetle doğru orantılıdır. Algılayıc bu doğrusal değişimleri kullanarak ölçüm yapmaktadır.

Piyezodirencin özelliğiyle üretilen bu algılayıcıyı, literatürdeki diğer basınç algılayıcılardan ayıran en önemli özelliği, yükseltmek amacıyla manyetik alanın kullanılmasıdır. Mıknatısla çekilebilen ve dirseğin uç kısmına yerleştirilen parçacıklar, mıknatıs etkisiyle efektif ağırlıkları arttırılarak ölçülmüştür. Bu sayede 20 mg aralıklarla ölçümü yapılabilen ağırlıklar 0.3 mg aralıklarla ölçülebilir hale gelmiştir.

Hassasiyeti 0.3 mg olan bu algılayıcı manyetiksel olarak aktif maddelerin ağırlığını ölçebilmektedir ve biyoalgılayıcıya kolaylıkla dönüştürülebilmektedir. Yapılması gereken tek şey MNP (manyetik nano parçacıklar)'ın biyolojik/kimyasal elementlere bağlanarak manyetiksel olarak aktifleştirilmesidir. Bu aktifleştirme işleminden sonra bir solüsyondaki biyolojik/kimyasal parçacığın ağırlığı ölçülebilmektedir.

TABLE OF CONTENTS

LIST OF FIGURES

LIST OF TABLES

LIST OF SYMBOLS/ABBREVIATION

Ɵ	Bending angle
F	Applied Force
L	Length
E	Young's modulus
I	Moment of inertia
x	Displacement
k	Spring constant
w	Width
t	Thickness
L_c	Length of cantilever
w_c	Width of cantilever
t_c	Thickness of cantilever
̊C	Centigrade
Q	Diameter
D	Design
ρ, σ	Resistivity
A	Cross-section area
$R_{PR}(\varepsilon)$	Piezoresistance
$\Delta R_{PR}(\varepsilon)$	Resistance change
ΔL	Length change
G	Gauss factor
ε	Stress
ε_{max}	Maximum stress
M(x)	Moment
Ω	Ohm
V_{out}	Output voltage
V_{in}	Input voltage
ΔV_{out}	Output voltage change
ξ	Constants

1. INTRODUCTION

1.1. MEMS DEVICES

The device of Micro Electro Mechanical System (MEMS) are divided into two groups; (a) sensors and (b) actuators. Sensors detect a specific input, such as light, gas, pressure, heat or force, from the physical environment to which it creates a response, mostly an electrical signal. Actuators, on the other hand, convert energy into movement which are mainly used in motors, pumps, switches, robotic arms and valves [1].

MEMS Devices: Sensors and Actuators

Electrostatic

- Inertia Sensor
- Pressure Sensor
- Flow Sensor
- Tactile Sensor
- Parallel-Plate Actuator
- Comb-Drive Actuator

Thermal

- Thermal Expansion
- Thermal Couples
- Thermal Resistors

Magnetic Actuation

Piezoresistive

- Inertia Sensor
- Pressure Sensor
- Flow Sensor
- Tactile Sensor

Piezoelectric

- Inertia Sensor
- Acoustic Sensors
- Flow Sensor
- Tactile Sensor
- Surface Elastic Waves

Figure 1.1. Schematic of MEMS Devices [2]

As seen in Figure 1.1, regarding their sensing and actuating principles, MEMS devices can be divided into mainly five distinct groups. These groups are (i) electrostatic [3] [4], (ii) thermal [5] [6], (iii) magnetic [7], (iv) piezoresistive [2] [8] [9] and (v) piezoelectric [10].

Electrostatic sensors are to measure the increase of capacitance which occurs between two oppositely charged conductors [11] [12]. **Electrostatic actuators**, on the other hand, are induced by electrostatic force which is occurred as a result of interaction of the two oppositely charged conductors under the applied voltage [13].

Thermal sensors aim to detect the temperature change by using various sensing methods, and the most commonly used ones are thermal couples, thermal resistive sensors and thermal

bi-morph sensors. In *thermal resistive sensors*, a material, whose resistance is subject to changes in accordance with the temperature change, is used [14] [15]. *Thermal bi-morphs* are composed of two merged materials by their longitudinal axis. Their axis faces different amount of elongation due to their different material properties. Consequently, the structure bends to the side which lengthens less [16]. Lastly, as it is seen in Figure 1.2, *thermal couples* are formed of two wires of dissimilar materials which are situated closely on one side so that they are able to connect at a point. There occurs a temperature difference between the sensing (measuring) junction and the reference junction. This temperature difference creates currents [17]. Apart from this, **thermal actuation** happens when the change in temperature of the microscale devices or structures cause mechanical displacement or creates force as an output.
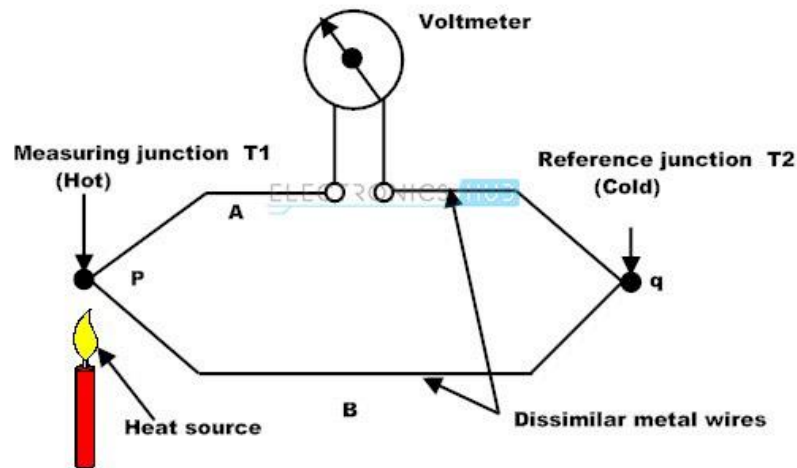
Figure 1.2. Thermal Couples [18]

Magnetic sensors generally use the magneto-resistive effect and the hall effect to measure the magnetic field. For **magnetic actuators**, permanent magnets or magnetic coils are mostly used to generate a moving force by creating magnetic field [7].

Piezoresistive sensors are made of piezoresistive materials. Their property called piezoresistivity makes the material to be subject to resistance change when the stress is applied [19] [20] [21].

Piezoelectric sensors exist by the virtue of some materials' properties such as Rochelle salt and quartz since those generate voltage or electric charge as a result of a mechanical

deformation [22] [23] [24]. And the opposite result is achieved by **piezoelectric actuator** since it transforms voltage or current change into mechanical deformation [25] [26].

Besides the types of MEMS devices, it is also important to examine the production of them. The primary material of MEMS devices is silicon [27]. It is used as a base material and since it is not flexible, chemical and mechanical etching can be applied for silicon slenderizing. However, those methods requiring advance fabrication techniques make the production process challenging. Additionally, the clean room equipment and laboratories are needed to produce and the manufacturing process can quickly escalate in complexity. As a consequence, the costs of silicon-based devices increase significantly.

New alternative to silicon-based MEMS device is paper-based design which enables to eliminate the disadvantages of silicon. Paper is lightweight, ubiquitous and easily disposable by incineration. It is flexible and can be easily shaped by laser cutter. Moreover, the manufacturing process of paper-based devices is faster, simpler and more inexpensive since it does not require clean room facilities and complicated fabrication techniques.

The advantage of paper was recognized in early twenties. One of the most important development in paper usage is the start of using filter papers in analyze laboratories. The novelty of filter paper is its contribution to acquirement of reliable results with a trace amount of sample. The filter paper was firstly produced by Martin and Synge in 1952 [28] [29] and it was used in the significant research of Whitesides *et all* which is called P-ELISA(Paper-based Enzyme-Linked Immuno Sorbent Assay) [30]. ELISA as a quantitative measurement technic was known and used by other scholars to detect the antigen or antibody. Following the method, a sample is put in a solution including antigen or antibody and if a reaction occurs, it is detected that the other particle, antigen or antibody, exists in the sample as well. [31]. P-ELISA is based on same principle but filter paper is used as a base so the samples and solutions are dripped on the filter paper. Consequently, the detection is achieved with a trace amount of sample and it prevented the waste of the products. The technic has led to other projects which use the cellulose based materials to detect the biological or chemical molecules.

Moreover, the advancement in biosensors by paper usage has been reflected to MEMS field. In last decades, cellulose base materials have been successfully adapted to MEMS actuators and sensors as a main production material. Since cellulose-based materials are disposable and low-cost, their usage as a base in MEMS device has increased significantly [32]. Additionally, the production process of paper-based devices does require neither as much labor force, nor as high qualification to produce as microfabrication technics.

One of the prominent instance of the usage of paper-based MEMS device is conducted by Martinez *et all* by developing a pneumatic actuator. In the research, both elastomer (Ecoflex) and easily bendable sheet are used to generate actuators. These actuators with pressurization are capable of complex motions which cannot be achieved by hard robots [33]. A different paper based actuator is developed by Hamedi *et all*. The actuator in this research is activated via electric and it is called HEPAs (Hydroexpansive Electrothermal Paper Actuators). With various configuration of paper and PEDOT: PSS composite, four types of HEPAs (straight, pre-curved, creased-curved and creased-sawtooth) are produced. The Figure 1.3 shows the types of HEPAs and their movements [34].
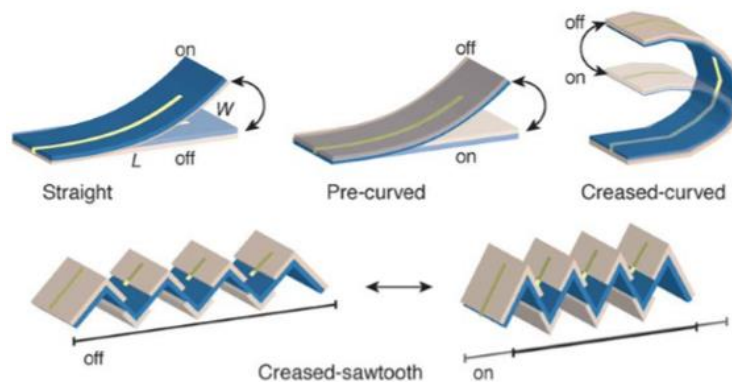
Figure 1.3. HEPAs types and their on/off positions [34]

Paper-based MEMS devices also include sensors, one of which is the microfluidic device. µPEDs (Microfluidic Paper-based Electrochemical Devices) are one of the microfluidic devices which is produced only by adhesive tape, ink and paper. It is designed to detect for both glucose and heavy-metal ions [35]. Another paper-based sensor is capacitive touch pad. This pad is fabricated by metallized paper and double-sided tape. This structure functions as capacitive key and gives binary responses [36].

It is indicated by my literature search that there are several studies conducted to create paper based piezoresistive sensors. The similar trend has occurred resulting in the replacement of silicon with paper for a base of piezoresistive sensors. In one of the conducted research, chromatography filter paper is cut in a cantilever shape and graphite is used as a piezoresistor. This system's response is examined by Wheatstone bridge circuit and weight is measured with the limit of detection(LOD)/resolution as 15g/25mg. This sensor is produced by screen printing method with simple laboratory equipment in sixty minutes [37].

Similar sensor is made by Yang *et all*. The aim of this research is to eliminate the necessity of laboratory. An ordinary photocopy paper, a pencil (2B) and scissors are used. Despite the fact that it has a worse rate (20g/50mg), the sensor is managed to be produced faster (thirty minutes) without laboratory equipment [38]. Another piezoresistive pressure sensor is developed by Crowley *et all*. In the research, the wind velocity, which is equal or higher than 3m/s, is measured by the sensor [39]. The disadvantage of paper based sensors is their single-use characteristic. It has been eliminated by Bailey *et all* by using PEN (Poly Ethylene Naphthalate) to generate a disposable piezoresistive sensor. This sensor gives reliable results in up to hundred thousand tests [40].

In brief, the increased use of cellulose based MEMS devices can be traced back in time as the benefits of cellulose, such as low cost and easiness in production process, has been taken advantage of by scientists.

The benefits of cellulose based materials explained above are taken into consideration to develop this thesis as well. Various types of paper and PLA are taken benefit of to generate a weight sensor. Besides, the thesis takes the advantage of piezoresistive materials to contribute the production of the sensor. As explained below [*see* section 1.3], resistance of piezoresistive materials, such as graphite, doped-silicon and germanium, change under mechanical deformation caused by applied stress. This property provides opportunity to measure the electrical response of applied force. In addition to that, graphite has an easiness in implementation which makes it a prior choice. Therefore, in this thesis, graphite is utilized as a piezoresistor. The material property of graphite is explained more detail in section 3.2.

1.2. BIOSENSORS

Biosensor as a terminology in science was first appeared in 1977 with the development of a sensor composed of an enzyme and an electrode and hence, called as a biosensor [41]. The main function of a biosensor is to measure the electrical response of biological reactions [42] [43]. As seen in Figure 1.4, in the older type of biosensor, there are only two main parts. One of them is called receptor which collects the required particles in the mixed solution and based on the reaction of these particles, it sends signals to transmission [44] [45]. These signals are transformed into readable electrical responses by the converter. Both transmission and converter form the second part of the biosensor called transformer.
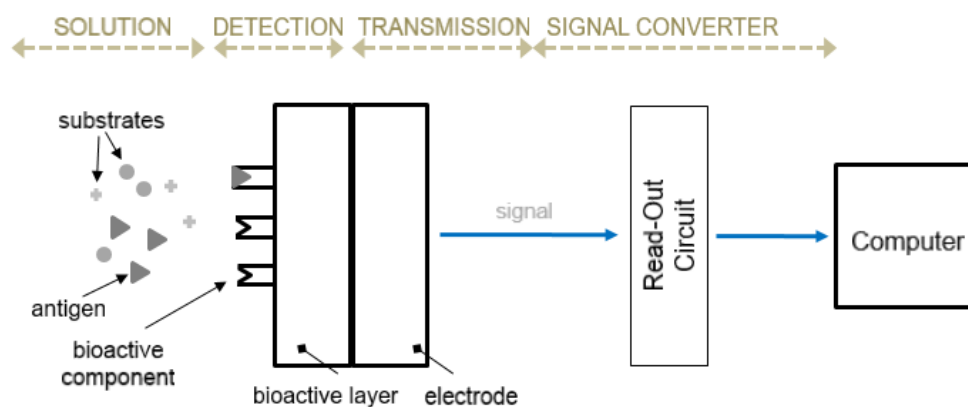
Figure 1.4. Structure and Operation Principle of Biosensors

In the present, biosensors are developed with three main parts instead of two to increase the reliability of detection and to decrease the signal noise ratio (SNR). In addition to receptor and transformer which are traditional biosensor parts, reference element is added as a third part [41]. Different to the receptor, reference element does not include any biological particles and hence, no biological reaction takes place. The purpose of this element is to eliminate the effects of the environmental conditions or the minor device problems.

Biosensors can be examined under five groups based on bioactive layer-transmission and detection methods. As it is seen in Figure 1.5, these groups are (a) electrochemical in other words amperometric [46] [47], potentiometric [48] [49], voltametric [50] [51], voltamperometric [52] and conductometric biosensors [53]; (b) piezoelectric based biosensors [54] [55]; (c) calorimetric in other words thermistors [56] [57]; (d) piezoresistive

biosensors [58] [59] and lastly (e) optic based namely photometric [60] [61], fluorometric [62] [63] and bioluminescence [64] [65] biosensors.

BIOSENSORS

Electrochemical	Piezoelectric	Calorimetric	Piezoresistive	Optical
• Amperometric • Potansiometric • Voltammetric • Voltamperometric • Conductometric		• Thermistors		• Fotometric • Fluorometric • Bioluminescence
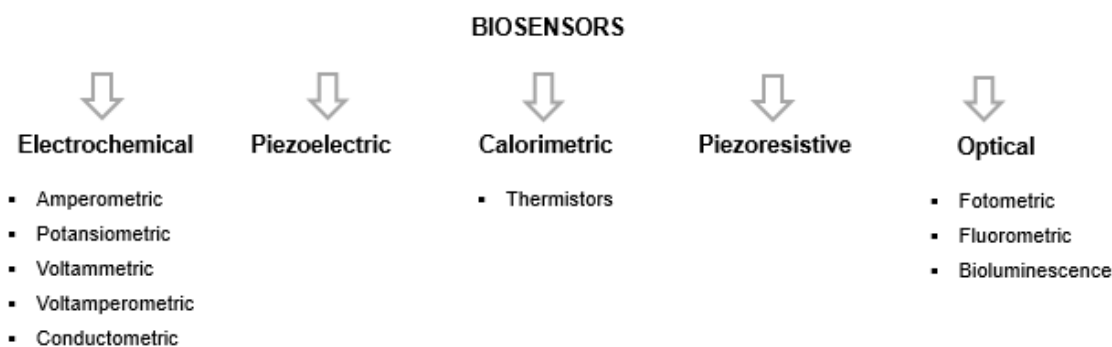
Figure 1.5. Classification of Biosensors

In literature, the first *amperometric sensor* was generated by Prof. L.C. Clark Jnr. in 1956, then it was called as biosensor regarding its properties [66]. This biosensor which is called Clark Electrode is used to detect the oxygen level. Clark Electrode and other amperometric sensors mainly measure the current that occurs in accordance with the number of electrons. these electrons release due to the chemical oxidation reaction or reduction reactions in the electrochemical cells. In present, amperometric biosensors are still used as blood sugar detection devices. Alternatively, *potentiometric biosensors* are produced in the literature. This kind of sensors detects the changes in potentials of electrodes without applying additional voltage. Changes in potential occur in the electrochemical cells because of the chemical reaction of the electrodes [46]. The research conducted by Rechnitz *et all* can be given as a prominent instance of use of potentiometric biosensors in which they successfully measured the amount of urea by urease hydrolysis [46].

Other group of biosensors is optic based sensors whose mostly known example is Surface Plasmon Resonance (SPR). This type of sensor was firstly used by Liedberg *et all* to observe the real-time interaction [67]. In 1990, BI Acore, which is based on SPR principle, was produced and released by Pharmacia company [68]. The operation principle of SPR biosensors is briefly shown in Figure 1.6. In the SPR-based biosensors, when biochemical reactions on the sensing surface change the refraction index, the resonance angle and SPR are impacted. The resonance is created as a result of optical excitement on the interface between the conductive metal membrane and dielectric material. Hence, the ratio of

biological elements in the sample is sensitively quantified. Another optic based biosensor is brought out by Lubbers and Opitz [67]. They produced a *fiber-optic biosensor* which was called Optode. It quantifies the amount of oxygen and carbon dioxide which is released as a result of oxidase reactions [42].
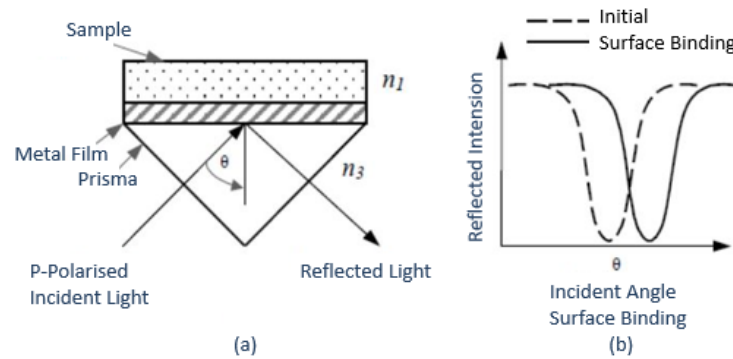
Figure 1.6. Operation Principle of SPR Biosensors (a) three layers' geometry for excited surface plasmon. A surface plasmon wave is excited in the metal interface. (b) SPR reaction [48].

Distinct from the groups based on the bioactive surface and measurement methods as shown in the Figure 1.5, the biosensors can also be grouped based on the relation of particles and their bioactive components. Under this method, three groups can be set, which are (1) biocatalytic (microorganism and enzyme used) biosensors, (2) microbe based biosensors and lastly (3) bioaffinity (antigen/antibody or receptor/ligand alike interaction used) biosensors [45]. The first biosensor of the biocatalytic group was produced in 1964 by Yahiro *et all*. In the sensor, the glycose/O2 is used as a fuel cell catalyst as well as an enzyme in the biofuel cell [69]. The idea of merging antibody to piezoelectric or potentiometric sensors leads to biocatalytic based biosensors. Ishiguro *et all* produced a biocatalytic sensor and published the related article in 1976 [70]. In the same year, another biosensor was produced by using a microbe which was the first of the second group of biosensors, namely microbe based biosensors [71]. The corn microbe was used to measure the rate of mutation of a corn which was due to the plant killing chemicals.

The aim of the thesis has been to generate a piezoresistive weight sensor which is to be used in production of piezoresistive biosensors in the further steps of the project. This potential sensor is planned to be part of bioaffinity group that can get benefits from the relation between the antigen-antibody. In the concept of this thesis, cellulose based piezoresistive

weight sensor is produced by fast and easy fabrication methods. In the further steps, it is planned that instead of measuring weight, the biological particles will be detected and quantified by using it as a biosensor. The sensor can be used to detect biological and chemical particles like cells, aflatoxin and DNA.

1.3. METHODOLOGY

The primary aim of this thesis as mentioned below is to generate a weight sensor which can be adapted as a piezoresistive biosensor. The biosensor will be basically composed of a paper-based microstructure, a read-out circuit and a magnet as depicted in Figure 1.7. This biosensor will recognize the existence and/or measure the amount of the biological/chemical particles.

The operation principle of the piezoresistive biosensor relies on the ELISA method of antigen/antibody. In the ELISA method, the key lock behavior of antigen and antibody is used to detect the antigens. Antigens bind only a specific antibody and the detection methods get benefits from this property. The antigens are marked with gold or latex nano particles. These particles are observable colors under the microscope. When the sample is mixed with the antibody solution, antigens and antibodies are bond to each other. Antibodies are mostly used to get rid of the unnecessary particles that the sample includes. Then, only marked antigens with antibodies are stayed. Under the microscope, the color concentration is observed to the amount of gold or latex particles which are equal to the amount of antigens.

In contrary to traditional ELISA method, in the furtherance study, the piezoresistive biosensor gets benefits from the magnetic nano particles (MNP). Instead of the gold or latex nano particles, MNP will bound to antigens and the number of them will be equal to the antigens. MNP is a magnetically active particle since it includes iron atoms. When the magnetic amplifier is active, the existence of MNP provides to increase the effective mass of biological component that is mainly composed of antigen, antibody and MNP and may also include additional biological particles like protein. The magnetically active component is pulled down by the magnetic amplifier since the amplifier creates a magnetic field with the help of magnet/electro-coil. Therefore, the magnetic amplifier is worked like increase in gravitation. This increase also causes an increase in effective mass of biological component

that makes the weight measurement possible with the paper based piezoresistive weight sensor.

Achieving this sensor is the main aim of this thesis and its working principle depends on the property of piezoresistive material. As shortly mentioned above, this kind of materials like graphite is sensitive to stress. The stress is occurred by the mechanical deformation which is caused by applied force. In substance, the applied force increases the stress level which is affected the piezoresistive material. The response of the piezoresistive material to the stress is to change the value of its resistance. This change is directly bonded to the applied force which is created by the interaction of biological component and the magnetic amplifier and its amplitude is linearly related to the amount of the biological component. Therefore, the value in resistance change of piezoresistive material corresponds to the amount of biological component.

In order to achieving the detection of biological/chemical particles with weight, two different weight sensor device is prepared. In the first device (piezoresistive weight sensor without magnetic amplifier), there are three components; read-out circuit, cantilever and weight plate as seen in Figure 1.7. First component, the read-out circuit is composed of power supply which provides input voltage of the circuit, digital multimeter that is necessary to measure the output voltage of the circuit and the Wheatstone bridge which is essential to eliminate the environmental impact on the output voltage. Second component, the cantilever that can be also named as weight sensor includes paper base, graphite coated area (piezoresistive layer/piezoresistor) and silver coated area (contact pad). Third component, weight plate, a place to put the weights that are to be measured, is tied by a rope to the free end of the cantilever.
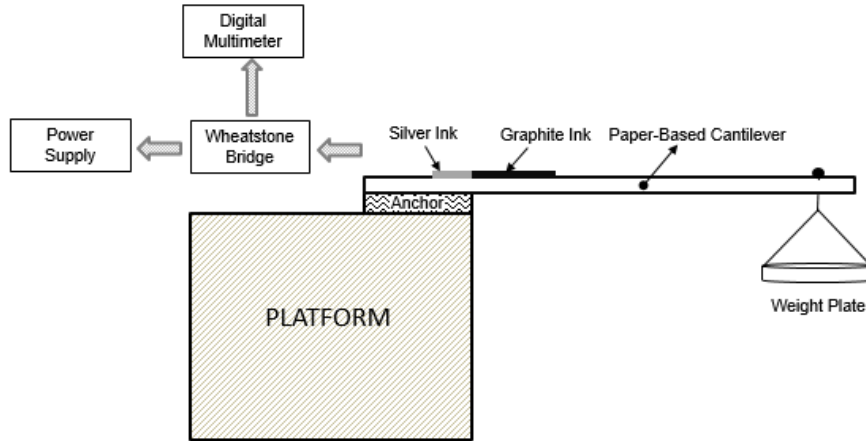
Figure 1.7. Schematics of proposed weight sensor.

Besides the components of weight sensor device, it is also important to examine the relation of the components with each other. When the weight is put into the weight plate, the rope pulls down the free-end of the cantilever. The free-end of cantilever bends as much as the amount of the weight. This bending cause mechanical deformation which increases the amount of stress that occurs in the fixed-end of the cantilever. The higher level of stress changes the value of piezoresistor which is located on the surface of the paper based as seen in Figure 1.7.
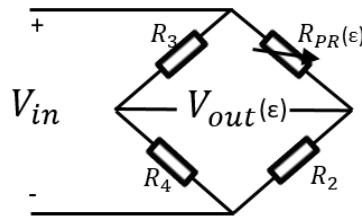
Figure 1.8. Wheatstone Bridge Circuit

The piezoresistor is connected to the Wheatstone bridge and this connection is provided by the silver contact pads. The connection is seen in Figure 1.8. The relation between the $R_{pr}(\varepsilon)$ and the $V_{out}(\varepsilon)$ is given in Equation 1.1.

$$V_{out}(\varepsilon) = \left(\frac{R_2}{R_2+R_{PR}(\varepsilon)} - \frac{R_4}{R_4+R_3}\right) V_{in} \qquad (1.1)$$

$R_{pr}(\varepsilon)$ represents the piezoresistor, which changes its value with the stress ε, where $V_{out}(\varepsilon)$ represents the output voltage and V_{in} is the input voltage. Regarding this equation, the value

of output voltage is inversely proportional to the value in resistance change of piezoresistive layer. As a consequence, the value in output voltage change which is measured by digital multimeter is proportional to the amount of the weight.
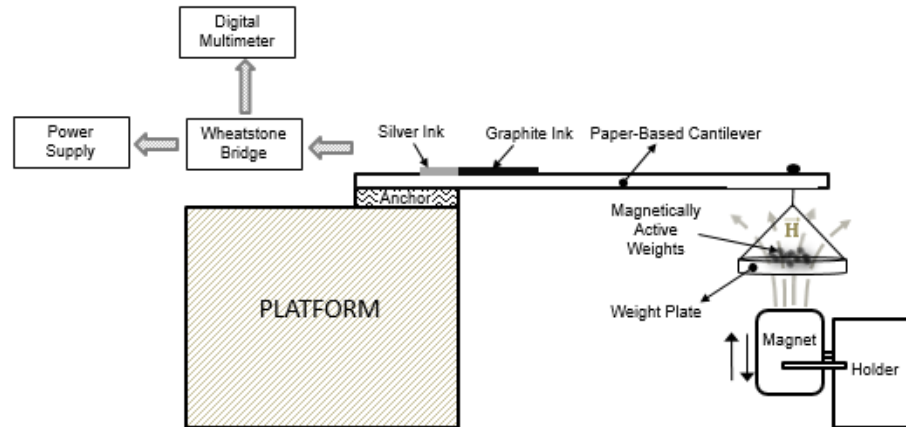
Figure 1.9. Schematics of proposed weight sensor that uses the magnetic mass increase scheme

In the second device (piezoresistive weight sensor with magnetic amplifier), on the other hand, there are four main components as seen in Figure 1.9. The three components are same as the first device and also their interaction. Fourth component comprises of a magnet and a holder which provides z-axis movement to the magnet, in other words, up and down displacement. The fourth component is called as magnetic amplifier. As mentioned above, magnetic amplifier increases the effective mass of the weight that is put into the weight plate, when the weight is magnetically active. Hence, this device can be only used for the weights which can be pulled down with magnet. At first, the magnet touches the weight plate, then the holder pulls down the magnet until the maximum displacement occurs that the force between the weight and the magnet counterbalances the endurance force of the cantilever to the bending. Therefore, the interaction between magnetic amplifier and the weight provides more bending compare to the weight provide itself.
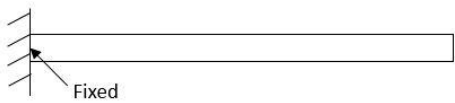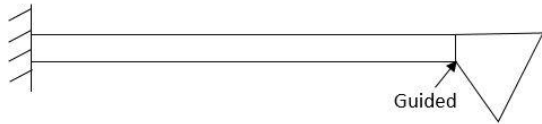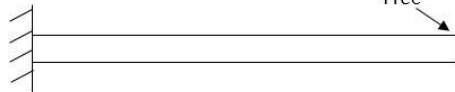
Furthermore, addition to these two devices, in this thesis, two distinct printers are modified to print protein and silver ink. In the further studies of the project, for converting the device to the biosensor device, free-end of cantilever is coated by albumin to fasten the biological components to the cantilever. Therefore, the printer for protein printing is necessary where the silver printer is modified to improve the fabrication process. The details about the printer modification is mentioned at Appendix A.

2. MECHANICAL DESIGN AND SIMULATIONS

2.1. CANTILEVER MECHANICS

Beams are usually classified based on three boundary conditions: fixed, guided and free. Each of them has different degrees of freedom (DOF) [2].

Table 2.1. Relation between the boundary conditions and the degree of freedom.

Boundary Conditions	Linear DOF	Rotational DOF
Fixed	0	0
Guided	2	0
Free	2	1

The fixed end does not allow any kind of movement whereas the guided end only restricts the rotational DOF and allows the two linear DOF. The free end has the highest DOF with two linear and one rotational.

Combinations of boundary conditions are utilized for both generation of the flexural beams and the classification of them. In MEMS field, mostly the fixed-fixed (bridge), fixed-guided and fixed-free (cantilever) beams are used.
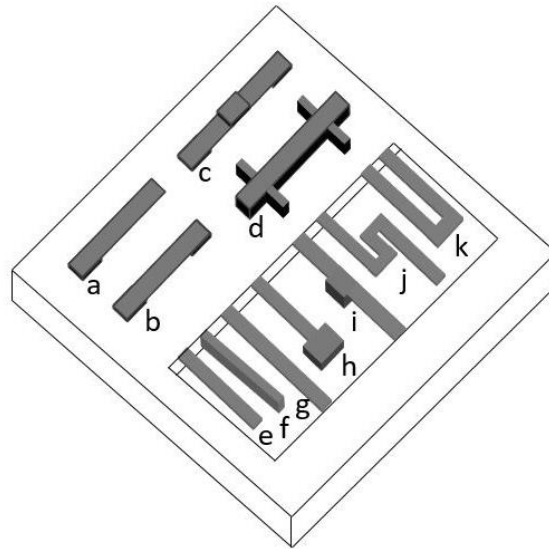
Figure 2.1. Flexural beams of different combination of boundary conditions

Figure 2.1 shows the various beam types, the most common ones in the MEMS fields. The beams are (a) a fixed-free cantilever parallel to the surface of the substrate, (b) a fixed-fixed beam parallel to the surface of the substrate, (c) two fixed end and guided boundary condition in the middle beam, (d) four fixed-guided beam connect to a rigid shuttle, (e) a fixed-free cantilever, (f) a fixed-free cantilever (the design allows the movement within the substrate), (g) a fixed-fixed beam, (h) a fixed-free beam with an object that restrict the flexural bending, (i) a bridge with the guided object in the middle, (j) a combination of several fixed-free cantilevers, (k) two fixed-free cantilevers connected in parallel [2].
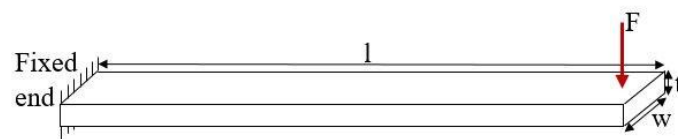
Figure 2.2. A fixed-free beam with dimensions l, w, t under applied force (F).

Fixed-free beams are called cantilevers and have two linear freedoms. First one is perpendicular to the fixed end (both up and down) and the second one is parallel to the fixed end (both left and right). In addition, cantilevers have rotational freedom thanks to their free end [2].

When the F magnitude of force is applied on the direction of the z-axis (Figure 2.2), the bent angle can be calculated by using the following equation

$$\theta = \frac{FL^2}{2EI} \qquad (2.1)$$

where the bent angle depends on force (F), length (L), Young's modulus (E) and moment of inertia (I). Calculation of the displacement in the z-axis is calculated by same parameters, but the equation is

$$x = \frac{FL^3}{3EI} \qquad (2.2)$$

The spring constant (k) is also an important factor for cantilever designs and analysis. The k variable can be calculated by use of Equation 2.3, where width is w, the thickness is t.

$$k = \frac{F}{x} = \frac{3EI}{L^3} = \frac{Ewt^3}{4L^3} \qquad (2.3)$$

These equations are the simplified formulas that analyze cantilever behavior. In this thesis, the comsol simulation program is used to analyze the displacement and stress characterization of the cantilever.

2.2. MICROSTRUCTURE DESIGNS

The cantilever is the most common beam type. They are mostly preferred thanks to their ease of fabrication and their usefulness, which is because cantilever design is simple and reliable that can be easily modified for different purpose and setups. Therefore, in this thesis, cantilever is preferred. The most important point of generating the device is to maximize the sensitivity of the sensor. It is analyzed by the relative change in the value of resistance as a result of the change in magnitude of applied force. It also aims to eliminate the environmental effect from the change in resistance and hence, reach more reliable results. Therefore, four different cantilever design are designed and shown in Figure 2.3. Each of design with various dimensions is simulated by Comsol software.

First design has an advantage in the fabrication process due to the dimensional limits of our fabrication method (Figure 2.3.A) whereas the expected advantage of second design is to increase the amount of displacement under the applied force (Figure 2.3.B). The third design, moroever, is a serpentine cantilever which increases the movement capacity of free end (Figure 2.3.C). The fourth design (Figure 2.3.D) is beneficial from many aspects. Connecting piezoresistor in series enables the total change in value of resistance in piezoresistive layer to increase and hence, the sensitivity of the sensor can be improved. Additionally, it provides opportunity to implement differential measurement by including more than one piezoresistances.
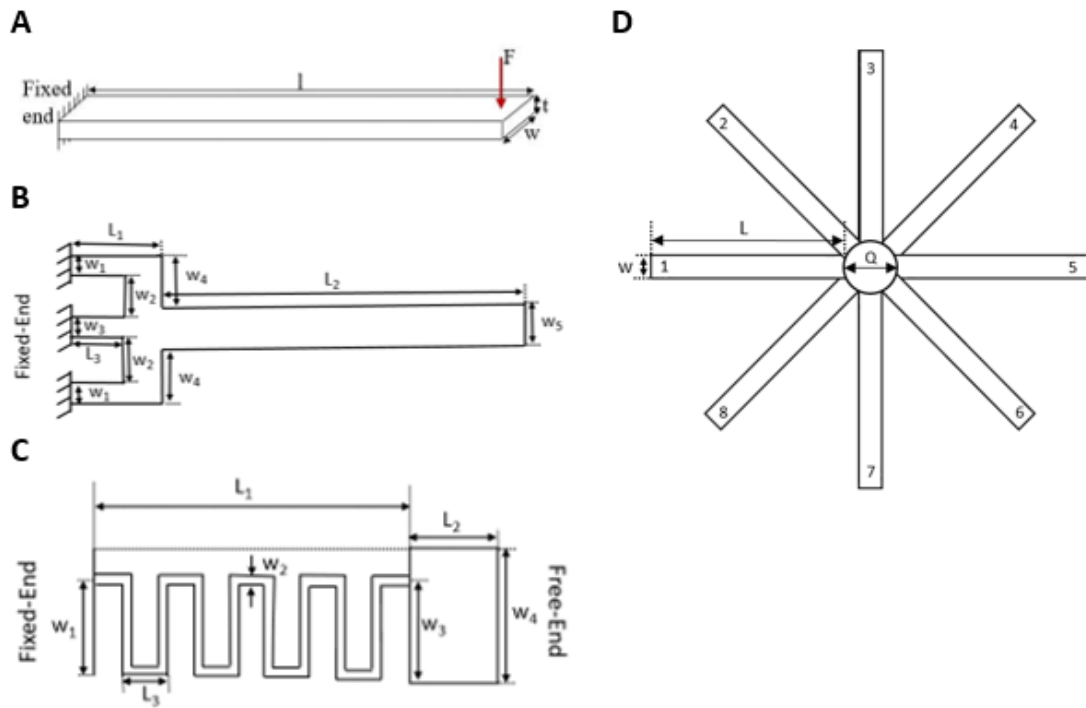
Figure 2.3. Microstructure designs with various dimensions. (Dimensions are shown in Table 2.2,2.3,2.4,2.5)

In the design under Figure 2.3 (A), eight different cantilevers are designed to identify the effect of change in width and length of cantilevers. When the length is kept constant, the width is changed to observe the effect of width on the values of displacement and stress. To the contrary, the width is kept constant while the length is changed to observe the effect of length.

Table 2.2. The basic designs with dimensions; width (w), thickness (t) and length (l). The parameters are given in μm range.

	w	L	t
1	8000	45000	88
2	6000	45000	88
3	4000	45000	88
4	2000	45000	88
5	1000	45000	88
6	2000	30000	88
7	2000	15000	88
8	2000	60000	88

In the second design under Figure 2.3 (B), eight different cantilever are designed to identify the effect of cross-section area. The fixed part of the cantilever is disintegrated into three parts as shown in the figure. Based on the parameters provided in Table 2.3, cantilevers are drawn.

Table 2.3. The fixed-free end designs with dimensions; width (w) and length (L). The parameters are given in μm range.

	w_1	w_2	w_3	w_4	w_5	L_1	L_2	L_3
1	1900	1000	1900	3000	1700	5000	40000	1000
2	1230	2000	1240	3000	1700	5000	40000	1000
3	1900	1000	1900	3000	1700	5000	40000	2000
4	1230	2000	1240	3000	1700	5000	40000	2000
5	1900	1000	1900	3000	1700	5000	40000	3000
6	1230	2000	1240	3000	1700	5000	40000	3000
7	1900	1000	1900	3000	1700	5000	40000	4000
8	1230	2000	1240	3000	1700	5000	40000	4000

In the serpentine cantilever design under Figure 2.3 (C), parameters are chosen to determine the impact of serpentine shape. Additionally, the chosen parameters give opportunity to observe the effect of both the width and the length of cantilevers.

Table 2.4. The serpentine designs with dimensions; width (w) and length (L). The parameters are given in mm range.

	w_1	L_2	w_3	w_4	L_1	w_2	L_3
1	1.5	5	1.5	3	15	0.1	0.3
2	1.5	5	1.5	3	30	0.1	0.3
3	1.5	5	1.5	3	15	0.2	0.6
4	1.5	5	1.5	3	30	0.2	0.6
5	1.5	5	1.5	3	60	0.2	0.6
6	1.5	5	1.5	3	25	0.5	1.5
7	1.5	5	1.5	3	50	0.5	1.5
8	1.5	5	1.5	3	75	0.5	1.5
9	1.5	5	1.5	3	25	1	3
10	1.5	5	1.5	3	50	1	3
11	1.5	5	1.5	3	75	1	3

In the fourth design under Figure 2.3 (D), the cantilevers are drawn based on the chosen parameters to observe the amplitude of lost in displacement. The lost should be compared to the gain achieved by the series connection of piezoresistors. If it is acceptable or evitable, then this design will be preferred because it indicates that the sensor is more reliable.

Table 2.5. The fixed-free end designs with dimensions; width (W) and length (L). The parameters are given in μm range.
Existence of the cantilever is marked as X.

	W	L	Q	1	2	3	4	5	6	7	8
1	8000	45000	5000	X				X			
2	8000	45000	5000	X		X		X		X	
3	8000	45000	5000	X		X	X	X		X	X
4	8000	45000	5000	X	X	X	X	X	X	X	X

In the simulation part, the technical drawings for each design are prepared. The parameters of Figure 2.3 A, B, C and D are respectively given in Table 2.2, 2.3, 2.4 and 2.5. In the simulation, the force is applied to the edge which is located in the free-end. The magnitude of the force is equal to 1mN.

Stress and displacement results are simulated and accordingly, in Figure 2.4, 2.5, 2.6 and 2.7, maximum values of stress and displacement are given.
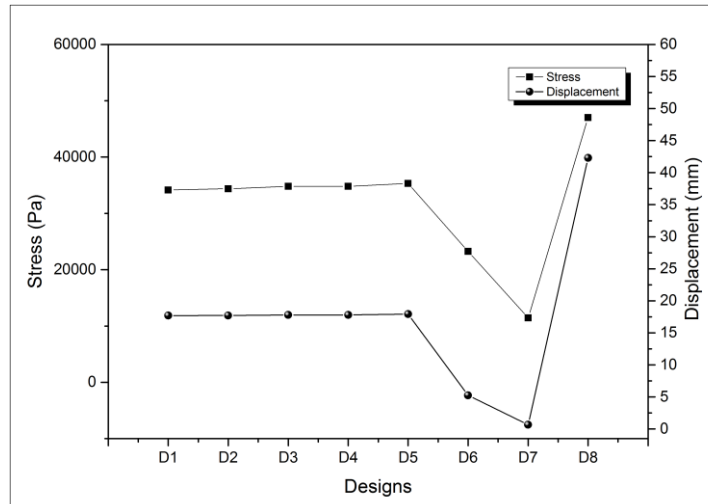
Figure 2.4. Simulation results of first cantilever whose parameters are given in Table 2.2

The simulation results of first design are shown in Figure 2.4. The graph points out that the length is more effective in maximizing the value of stress and displacement than the width. Hereby, the length should be maximized to generate the most sensitive sensor. Unfortunately, when the force is not applied, the cantilever cannot stay straight as it should and starts to bend as it lengthens.
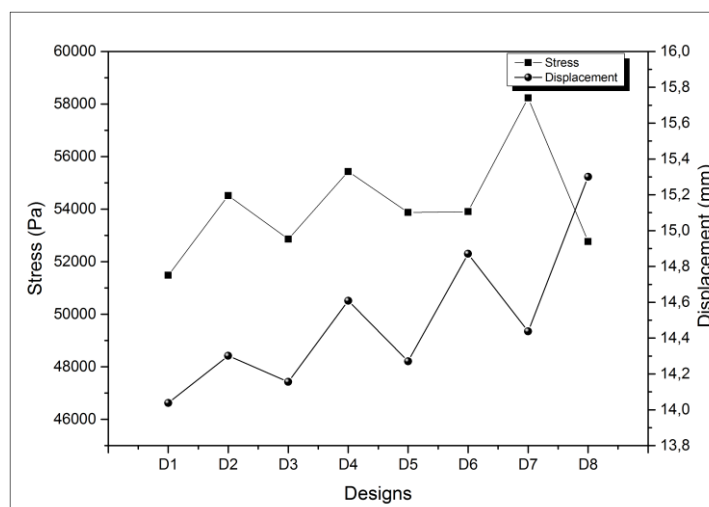
Figure 2.5. Simulation results of second cantilever whose parameters are given in Table 2.3.

The result graph of second design indicates that when the cross-section area is narrowed, the value of displacement and stress increases. Besides, it is indicated that the more the area extracted, the more cantilever bends.
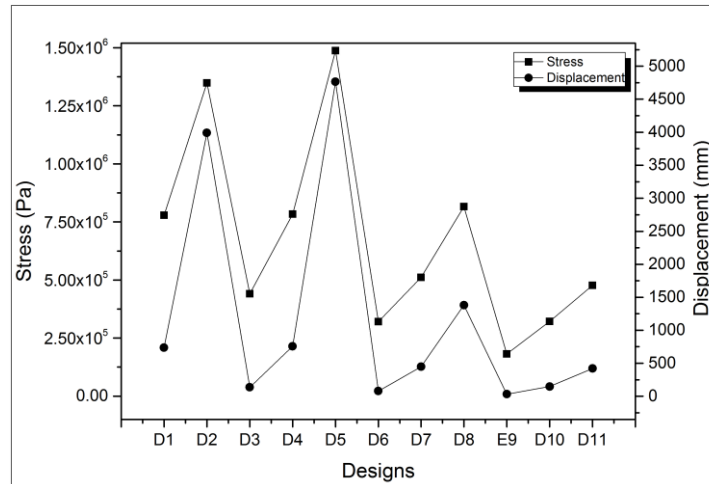
Figure 2.6. Simulation results of serpentine cantilever whose parameters are given in Table 2.4.

The result graph of serpentine cantilever points out that both width and length of cantilever have influence on the magnitude of displacement and stress. When the cantilever is narrowed or lengthened, the magnitude increases.
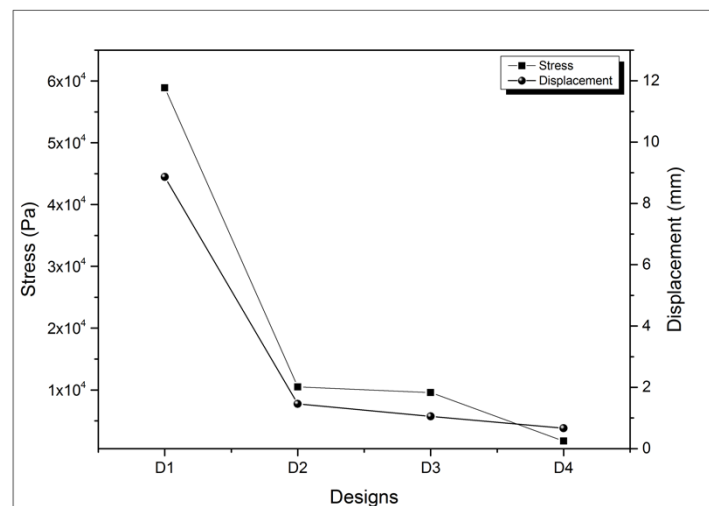
Figure 2.7. Simulation results of bridge structure whose parameters are given in Table 2.5.

The graph of bridge structure shows that the lost is neither evitable nor acceptable because each additional piezoresistor decreases the displacement value even more than it increases

the total change in the resistance. Therefore, this design cannot be preferred for the purpose of this thesis.

The results indicate that the displacement value of serpentine cantilever is the highest whereas the bridge design yields the lowest one. Although the serpentine cantilever seems as the best solution, the results may not be as reliable as others because its rotational movement causes inaccuracy in the values. Besides, its complexity makes the production process harder than the other designs. Regarding those facts, it has not become first choice in this thesis.

The displacement values of the first design (Figure 2.3 A) are not as high as the serpentine cantilever, however, it is acceptable and even selected as a cantilever shape since its fabrication process is easier. The graph indicates that the width of cantilever has a negligible effect on the values. Nevertheless, the length creates substantial difference. When the length is increased, the displacement increases as well. Due to the constraint explained above, the parameters cannot be selected in their maximum value. Hence, the drawing with the parameters 8 mm width and 45 mm length is the most suitable one. However, the dimensions are needed to be scaled by 0.79 to provide smaller sensor without changing the values. Thus, the new parameters are selected as 6,16 mm width, 35,6 mm length.
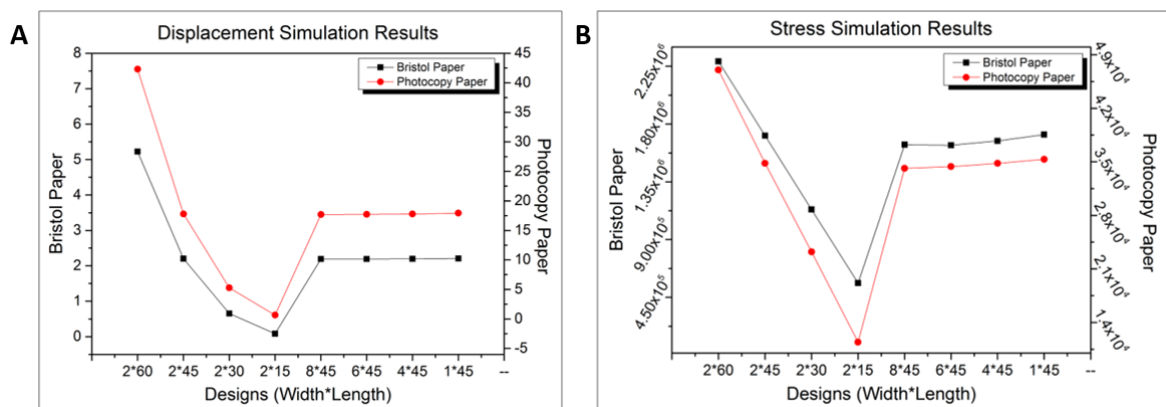
Figure 2.8. Simulation results of Bristol paper (400μm) and Photocopy paper (88μm) (A)Displacement of first design with various dimensions under 1N/m applied load (B)Stress of first design with various dimensions under 1N/m applied load

Even though the characterization of designs (cantilevers) are simulated with the properties of the photocopy paper, the cantilever is produced from Bristol paper. Therefore, the simulations for first design is repeated to observe whether the previous simulations and

assumptions are similar that can be used for fabrication without changing or not. The simulation results for both maximum displacement and stress are given in Figure 2.8. The similarity of the curves points out that the length and width effect in both material is same. Therefore, the selection of the dimensions should be similar. Additionally, the new material enables to lengthen the cantilever, nevertheless, the length is preferred not to be changed. It is because addition of the weight plate causes the cantilever to bend if the length is elongated. Moreover, the first design with selected dimensions (6.16mm width, 35,6 mm length) is simulated to observe the values in displacement and stress under various applied force.
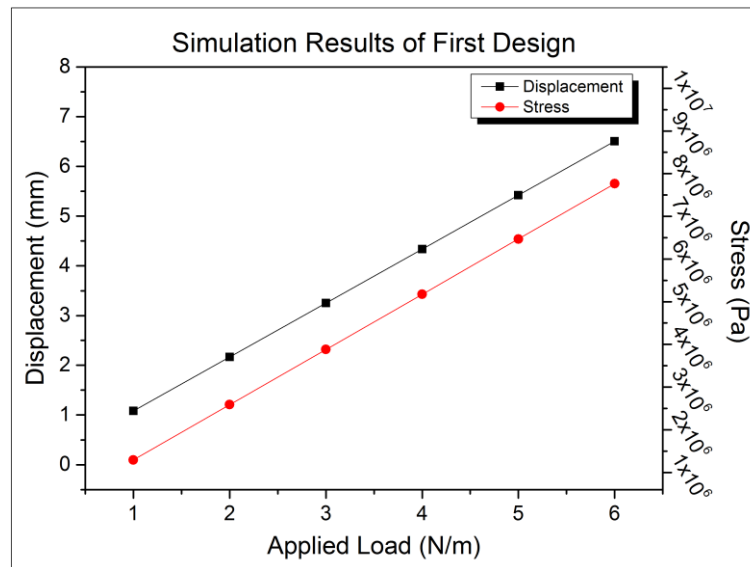
Figure 2.9. Displacement and Stress Graph of selected cantilever design where the properties of 400μm Bristol paper is used.

In Figure 2.9, the values in displacement and stress is given. The data indicate that displacement and stress level is linearly proportional to the applied force. Therefore, in the experiment, the results should be linearly proportional quantities if the weight is in the range of sensor.

3. ELECTRICAL DESIGNS AND CALCULATIONS

3.1. READ-OUT CIRCUITRY

3.1.1. Wheatstone Bridge Circuit

Piezoresistive materials are the most widespread material in the MEMS field, especially to fabricate sensors, however, their property of being temperature sensitive declines their ability to yield reliable results. Therefore, it has utmost importance to eliminate external temperature impact on the results [2]. Bridge configuration is the mostly used way to achieve this mainly because they are portable and easily adaptable. In bridge configuration, more than one resistance is used and since all resistances are impacted equally from the external temperature, its effect on the circuit design's output is managed to be restricted. The most commonly used bridge type for piezoresistive materials is the Wheatstone bridge circuit.

Wheatstone bridge is a circuit configuration with three resistances and a piezoresistance. It is effective to measure the values of the piezoresistances which are between 1Ω-$1M\Omega$ [72]. In other words, piezoresistances with values less than 1Ω or more than $1M\Omega$ cannot be measured accurately. Outside of the range, the sensitivity and the accuracy of the measurement decrease. In the range, however, the value of resistance can be measured with the margin of error being 0.1%.

$$V_{out}(\varepsilon) = \left(\frac{R_2}{R_2 + R_{PR}(\varepsilon)} - \frac{R_4}{R_4 + R_3}\right) V_{in} \qquad (3.1)$$

$$R_{PR}(\varepsilon) = R_2 \left[\left(\frac{V_{out}(\varepsilon)}{V_{in}} + \frac{R_4}{R_4 + R_3}\right)^{-1} - 1\right] \qquad (3.2)$$

In order to calculate the value of output voltage and the value of piezoresistance (R_{PR}), the Equation 3.1 and 3.2 can be used [2].

3.1.2. Optimization of Wheatstone Bridge

In an attempt to find the optimum values of resistance, calculations are completed. The governing equation for a Wheatstone bridge circuit is given in Equation 3.1 where $R_{PR}(0)$ is the initial resistance value of the unbent cantilever. One should remind that the magnitude of $R_{PR}(\varepsilon)$ is changing with the stress ε that occurs on the paper-based cantilever, same as the magnitude of $V_{out}(\varepsilon)$.

Our primary goal is to be able to detect minimum changes on $R_{PR}(\varepsilon)$, hence to increase the resolution of the proposed cantilever. This resolution improvement will make the measurement of milligram range weights possible. To be able to detect even the slightest change on $R_{PR}(\varepsilon)$, one should maximize the related change of $V_{out}(\varepsilon)$.

In order to maximize the magnitude of $V_{out}(\varepsilon)$, the term $R_4/(R_4+R_3)$ in Equation 3.35 should converge to zero. Therefore, the value of R_3 in Equation 3.1 should be maximized, whereas the value of R_4 should be minimized. For this reason, the magnitude of R_3 and R_4 are chosen as 1kΩ and 1Ω, respectively.

Assuming a negligible $R_4/(R_4+R_3)$ term; the relation between R_{PR}, R_2 and V_{out} is investigated using Matlab software tools. The relation of R_{PR} and V_{out} is depicted in Figure 3.2 (A), for different R_2 values. As it mentioned above, our main aim is to increase the sensitivity and the resolution of the sensor. Therefore, large value of ΔV_{out} and slope angle is necessary to be able to detect slight $R_{PR}(\varepsilon)$ changes (ΔR_{PR}). As it is seen in Figure 3.2 (A), the magnitude of R_{PR} is inversely related to the output voltage. Hereby the value of $R_{PR}(0)$ should be as small as possible. Additionally, small value of R_2 is required to have a large slope angle that facilitate the detection, whereas at the same time decreasing R_2 unlimitedly will create problems to fabricate small values of $R_{PR}(0)$.
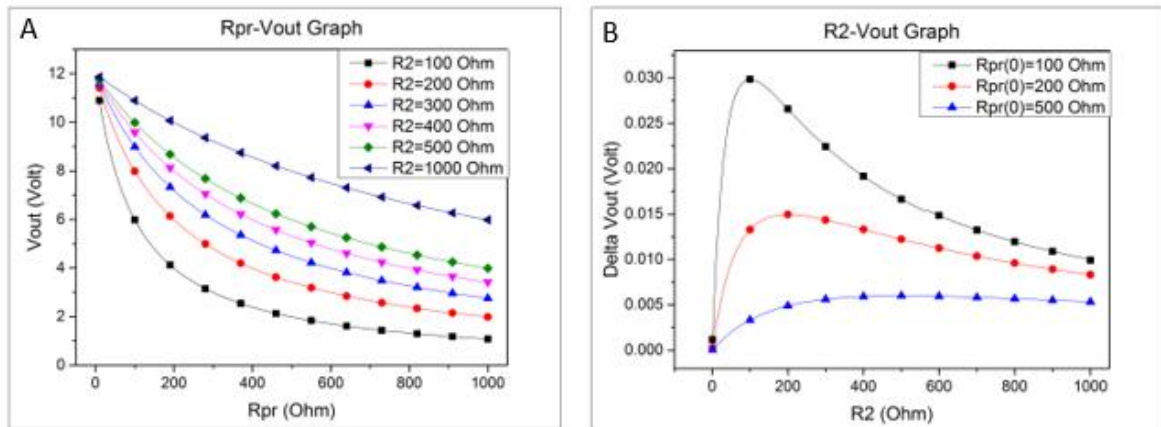
Figure 3.1. Wheatstone Bridge calculation graphs showing the relation between (A) R_{PR} -V_{out} and (B) R_2- V_{out}

In Figure 3.2 (B), ΔV_{out} versus R_2 plot is drawn for different R_{PR} (0) values, where $R_{PR}(0)$ is the initial resistance value of piezoresistor when there is no bending in the cantilever. The ΔV_{out} represents the output voltage difference between for 1Ω increase of a given R_{PR} (0). As it can be deduced from Figure 3.2 (B), the peak values of ΔV_{out} occurs where the values of R_2 and R_{PR} (0) are equal to each other.

In short, for the increased sensitivity, the slope of V_{out}-R_{PR} plot (dV_{out}/dR_{PR}) should be large, where the ΔV_{out} should be maximized. This means that R_2 should be small, while the initial value of R_{PR} (0) converges to R_2. Thus, the R_2 value should be preferred to be lower than $200 \ \Omega$.
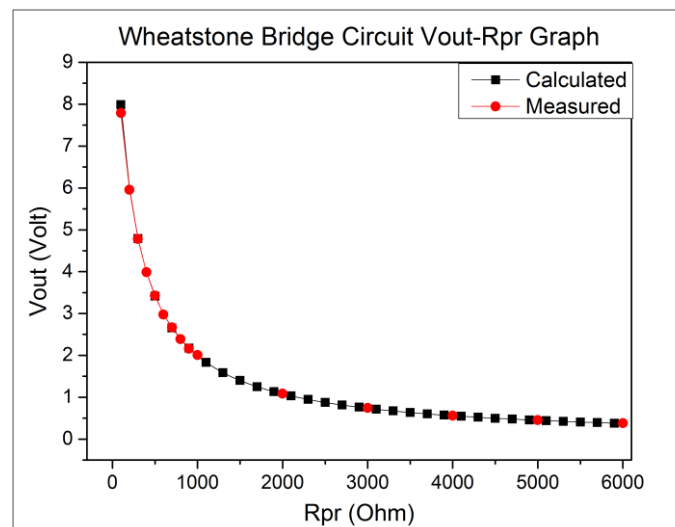
Figure 3.2. Comparison of theoretical and measurement results showing the relation between R_{PR} and V_{out}.

In order to compare the theoretical and experimental results, a Wheatstone bridge circuit is implemented. Using the Equation 3.1, the magnitudes of Vin, R_2, R_3 and R_4 are chosen as 12 Volt, 200 Ω, 1 kΩ and 1 Ω, respectively. The magnitude of V_{out} (0) is drawn for different R_{PR} (0) values in Figure 3.3. The plot indicates that the difference between the measurement results and expected ones are negligibly close to each other.

3.2. GRAPHITE

3.2.1. Material Property

Carbon atom is a non-metallic element which is located in 4A group in the periodic table. Its atomic number is 6 [73]. Carbon atoms can be bound to each other with different combinations and these distinct combinations create various products such as diamond and graphite. Despite of the fact that both are composed of carbon atoms, there is a strong distinction between diamond and graphite in their molecular structure. Diamond has a covalent lattice structure which makes it rigid and insoluble [74].
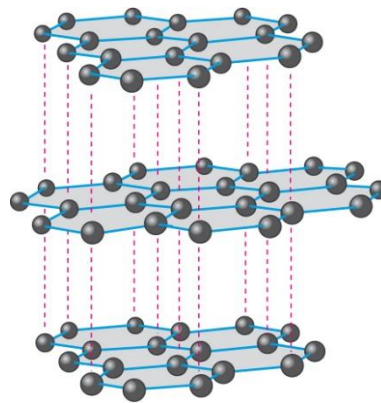
Figure 3.3. Graphite Molecular Structure [74]

In contrast, graphite has a strong hexagonal binding structure and a weak bond between the layers as shown in Figure 3.4 [74]. This structure makes graphite conductive and piezoresistive and consequently, the force can easily break the bonds between layers and make electrons free. Graphite is also soluble in water. These features enable graphite to be easily implemented on the paper. Additionally, graphite is accessible easily and with low cost. Therefore, it is the most suitable choice as a piezoresistor in this thesis.

3.3. PIEZORESISTIVITY

Value of piezoresistor faces a proportionate change with the amount of experienced strain. This property of piezoresistors provides rectilinear transduction mechanism between the mechanical and electrical domains.

The value of resistors is represented in the following equation where ρ is the resistivity, A is the cross-section area and L is the length of the resistor [2].

$$R = \rho \frac{L}{A} \tag{3.3}$$

Therefore, the value of piezoresistor changes dependently on both the dimensions of the resistor and the resistivity. The value of piezoresistor changes when a force is applied because the force has impact on stress level which has further impact on all of the variables in Equation 3.3. Firstly, force causes an increase in the length of the piezoresistor which, however, does not change the value itself. It is because the cross section area also increases under the force which helps keeping the value of piezoresistor approximately constant. The resistivity effect, to the contrary, changing under the applied force has a greater influence on the value. Therefore, the piezoresistor can be defined as the resistor whose resistivity value changes proportionately with the applied forced.

When it is defined in microscopic scale, the relation between the applied force and the change in the value of resistance is accepted linear being formulized as

$$G = \frac{\Delta R}{\varepsilon R} \tag{3.4}$$

where G is the gauge factor of a piezoresistor [2]. The gauge factor changes dependently on the material property and on temperature. In order to eliminate the temperature's impact on G, and hence on the resistor, the Wheatstone bridge circuit configuration is often used. In section 3.1, it is examined in detail.

It is further important to examine the increase of stress under the force applied. When there is pure bending, the only strain emanated is longitudinal. The force applied on a beam bends its axis into a curve (Figure 3.5). The plane passing from *nq* points is bent as a convex which causes elongation and tension. Besides, the upper part of the beam is bent as a concave which causes contraction and compression. Between the concave and convex part of the beam, there is a place left undistorted. This cross-section plane is shown as st-plane in the Figure 3.5 and called as neutral surface. If the beam is uniform, the neutral surface is located right in the middle. As the distance between an interior point and the neutral axis increases, the magnitude of stress increases with a linear proportionate which is a result of the symmetry and material homogeneity of the beam. Therefore, the maximum stress level is observed on the top or bottom surface of the beam which is equal for both tensile and compressive stress.
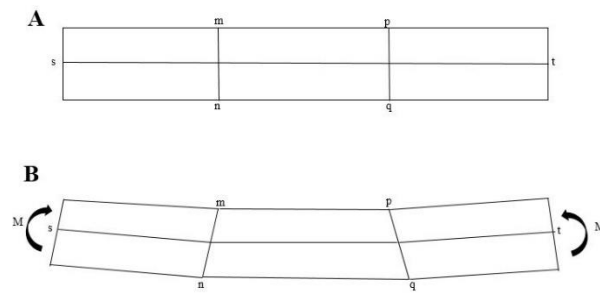
Figure 3.4. Longitudinal strain of the beam under pure bending.

Furthermore, for the cantilever design that is shown in Figure 3.6, it should be emphasized that the magnitude of the stress increases from free-end to fixed end. Hence, the maximum stress level is observed at the closest point to the fixed end.
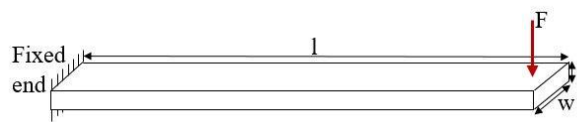
Figure 3.5. Free-end cantilever design under applied force (F) with dimensions l, w, t.

Based on two aforementioned results, the piezoresistive material should be implemented at a point on the surface and close to fix-end where the stress level is maximum. It is to increase the impact of the applied force on the resistance change.

The Equation 3.5 expresses the maximum stress in the cantilever, where M(x) is the total torque, E is the Young's modulus and I is the moment of inertia.

$$\varepsilon_{max} = \frac{M(x)t}{2EI} \qquad (3.5)$$

For the maximum torque, the maximum stress can be rewritten as

$$\varepsilon_{max} = \frac{Flt}{2EI} \qquad (3.6)$$

It is vital to state that the equation can only be used for calculations when the piezoresistive material is implemented in a layer whose thickness and length are negligible compared to the cantilever. Otherwise, the thick layer of the material itself becomes another source of stress which creates a need for a reformulation. The implementation of thin layer of the material also helps to simplify the fabrication process by requiring less material and time and simpler methods.

Moreover, when the material is implemented in a thick layer as in Figure 3.7 (C)/(D), sensitivity of the sensor decreases. The reason beyond is based on the existence of two opposite stress types: compressive and tensile. When the doped region passes the neutral axis of the cantilever as in Figure 3.7 (D), the total of tensile and compressive stress decreases. In an extreme case where the piezoresistor covers entire thickness of cantilever, the tensile stress and the compressive stress cancel each other.
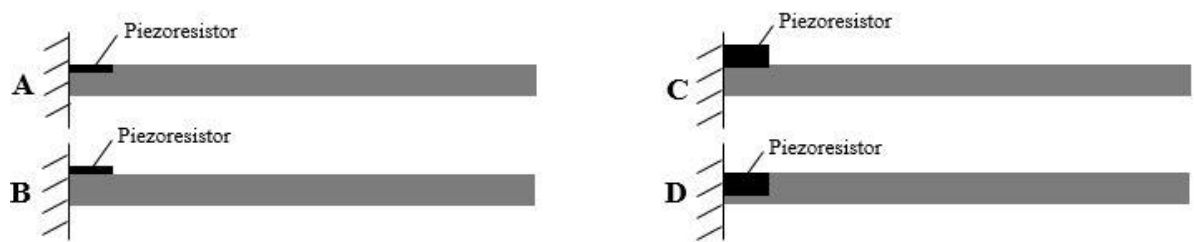
Figure 3.6. Cantilever with the piezoresistor (A) Thin layer of piezoresistor (doped) (B)Thin layer of piezoresistor (deposited) (C) Thick layer of piezoresistor (doped) (D)Thick layer of piezoresistor (deposited)

3.4. OPTIMIZATION OF PIEZORESISTOR

3.4.1. Heating

Graphite ink is in pasty form. It needs to dry after being implemented. In order to accelerate this drying process, a hot plate is used. An experiment is prepared to find the optimum duration for which five different conductive lines are produced with different width and length.

The conductive lines are placed on the hot plate. The degree is chosen as 60 °C since it is the degree of maximized heat which does not damage the products (paper, graphite and silver ink). The aim of maximizing the degree is to shorten the fabrication period. The values of resistances are measured every five minutes and the results are shown in Figure 3.8. The graph shows that after twenty minutes, the change in the values of resistances is minimal. On the other hand, waiting more than twenty-five minutes can cause damages. Therefore, the duration of heating is chosen as twenty minutes.
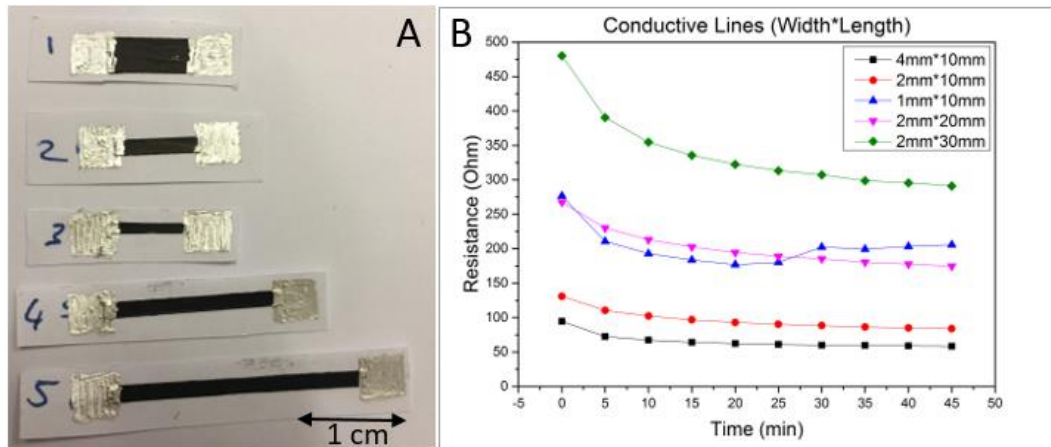
Figure 3.7. Heating Test of Graphite (A)Implemented graphite resistors on the cantilever for heating test. Dimensions of conductive lines are given with width and length respectively. (1)4mm*10mm, (2)2mm*10mm, (3)1mm*10mm, (4)2mm*20mm, (5)2mm*30mm. (B) Resistance-time graph of piezoresistors

3.4.2. Theoretical Work for Piezoresistance

The piezoresistor can be calculated by Equation 3.7 and the piezoresistor formula is given in Equation 3.7 where $\rho(\varepsilon)$, A_{PR}, L_{PR}, w_{PR} and t_{PR} are the piezoresistive layer's resistivity,

cross-section area, length, width and thickness, respectively. One should note that the magnitude of $\rho(\varepsilon)$ is changing with the stress that occurs on the fixed end of the cantilever.

$$R_{PR}(\varepsilon) = \rho(\varepsilon)\frac{L_{PR}}{A_{PR}} = \rho(\varepsilon)\frac{L_{PR}}{w_{PR}t_{PR}} \qquad (3.7)$$

In section 3.3, distribution of stress on the cantilever has been discussed. Stress under the pure bending increases towards the fixed end. Increased stress results in large resistance change on the piezoresistive material. Hence, the starting point of cantilever is the best location to implement the graphite.

In a piezoresistive layer, there are two types of stresses namely, tensile and compressive stress. These are reverse stresses that can be easily cancel each other. Thus, applying the piezoresistive material on the middle axis of the cantilever is undesirable. Moreover, one should assume that the thickness is negligibly thin compared to the thickness of the cantilever. Furthermore, the thickness is inversely related to the sensitivity of read-out circuitry. Resistance should be as small as possible to increase the sensitivity of Wheatstone bridge circuit, hence, piezoresistive layer should be thickened as much as the cantilever thickness tolerates. In line with these objectives, the thickness of graphite is planned to be 40 μm where the chosen paper thickness is 400 μm.

Additionally, the choice of dimensions of the piezoresistive layer is not only effected by the resistance change, but also by cantilever dimensions and property of read-out circuitry. All parameters and constraints are important for sensitivity and each of them is depended on the others. Therefore, the equation can be rewritten as below.

$$V_{out}(0) = \left(\frac{R_2}{R_2+R_{PR}(0)} - \frac{R_4}{R_4+R_3}\right)V_{in} \qquad (3.8)$$

The $R_{PR}(0)$ value in Equation 3.8 is an initial value of piezoresistor whose resistance is calculated by the Equation 3.7.

Assuming the following terms; $\frac{R_4}{R_4+R_3} \approx 0$ and $R_2 = R_{PR}(0)$, $V_{out}(0)$ in Equation 3.8 becomes equal to $V_{in}/2$ where the V_{in} is the input voltage.

If bending occurs, V_{out} changes and the Equation 3.8 transform as follows.

$$V_{out}(\varepsilon) = \left(\frac{R_2}{R_2 + R_{PR}(\varepsilon)} - \frac{R_4}{R_4 + R_3}\right) V_{in} \tag{3.9}$$

As we make the same assumption as in Equation 3.9, V_{out} becomes:

$$V_{out}(\varepsilon) = V_{in}\left(\frac{R_{PR}(0)}{R_{PR}(0) + R_{PR}(\varepsilon)}\right) \tag{3.10}$$

The difference between $V_{out}(0)$ and $V_{out}(\varepsilon)$ (ΔV_{out}) is given in Equation 3.11.

$$\Delta V_{out} = \frac{V_{in}}{2} - V_{in}\frac{R_{PR}(0)}{R_{PR}(0) + R_{PR}(\varepsilon)} \tag{3.11}$$

The magnitude of $R_{PR}(\varepsilon)$ is equal to

$$R_{PR}(\varepsilon) = R_{PR}(0) + \Delta R_{PR} \tag{3.12}$$

where

$$\Delta R_{PR} = \varepsilon G R_{PR}(0) \tag{3.13}$$

The Equation 3.13 can be transformed to

$$\Delta R_{PR} = \frac{FGR_{PR}(0)L_c t_c}{2EI} = \frac{FGR_{PR}(0)L_c t_c{}^4 w_c}{24E} \tag{3.14}$$

and the moment of inertia (I) is assumed as $12/(w_c t_c{}^3)$. In Equation 3.14, F represents the applied force, G is gauge factor, E is the Young's modulus. Additionally, L_c, w_c and t_c represent the dimensions of the cantilever.

$$t_c = 0.4\text{mm}; \quad L_{PR} = \frac{L_c}{5}; \quad w_{PR} = \frac{w_c}{3} \tag{3.15}$$

By using Eq. 3.12 and assumptions which are given in Equation 3.15, Equation 3.11 can be transformed to

$$\Delta V_{out} = \frac{V_{in}}{2} - V_{in} \frac{E\xi}{2EC + FGL_{PR}w_{PR}} \tag{3.16}$$

where the ξ is a constant and equal to 7.1 x 10^{-17}.

By using Equation 3.16, the theoretical results are calculated and given in Figure 3.8. The graph points out that the increase value of piezoresistive layer's width (w_{PR}) decrease the resistance changes and also sensitivity.
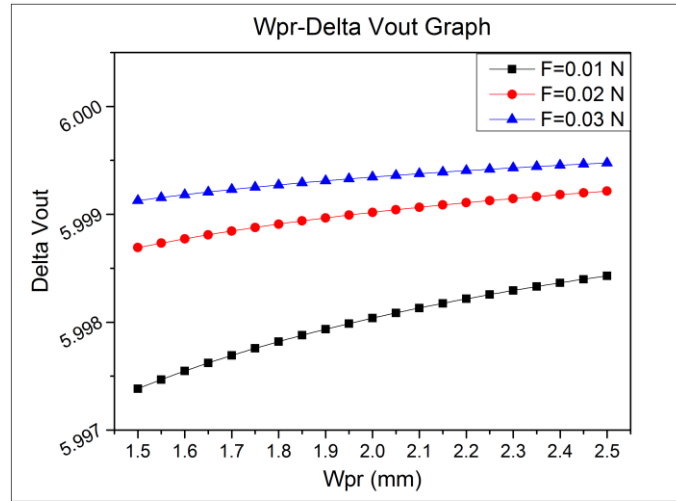
Figure 3.8. Theoretical Expression Graph of Width and Voltage Change

The Equation 3.16 is transformed as follow to be able to monitor the relation between the length and the width.

$$w_{PR} = \frac{1}{FGL} \left(\frac{2V_{in}E\xi}{V_{in} - 2\Delta V_{out}} - 2E\xi \right) \tag{3.17}$$

The Equation 3.17 indicates that length and the width is inversely proportional to each other. In Figure 3.9, the plot of Equation 3.17 is given, where the length and width is variable and the other parameters are constant. Input voltage and the change in output voltage is selected as their maximum values based on the circuit design. Their values are 12V and 1V,

respectively. The Young's modulus is chosen as 2,58 GPa which is the elastic modulus of the Bristol paper that is thought to be used. The range of Gauss factor is 5-15 for graphite ink, and 10 is chosen to be used in the graph. F is determined as 0.1 mN.
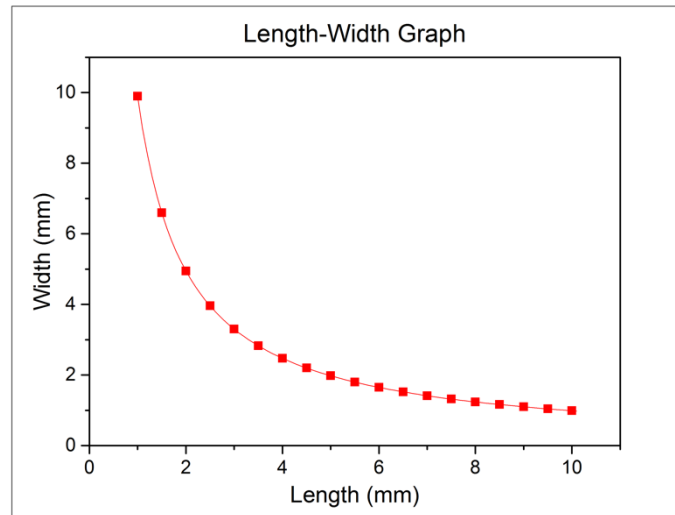
Figure 3.9. Mathematical Expression Graph of Length and Width

Furthermore, the graphite ink is electrically connected to the Wheatstone bridge circuit as mentioned previously. Therefore, the design should be like one of the shapes in Figure 3.10 to simplify the connection between the circuit and the piezoresistive layer. One should be noted that the aim is to minimize the length of the piezoresistor without increasing the width since it should be as small as possible for high-sensitivity values. Additionally, compared to the length of the cantilever, the length of piezoresistive layer should be negligible. Hereby, the designs in Figure 3.10 are preferred where the dimensions are chosen only to observe the characteristic of the shapes.
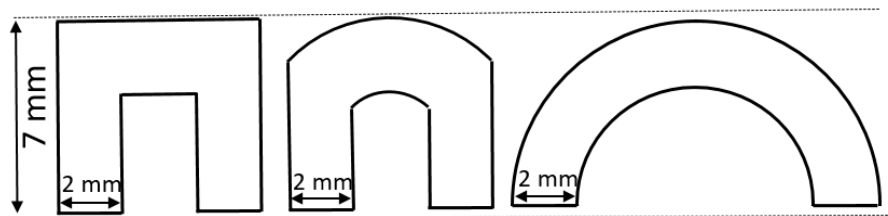
Figure 3.10. Alternative shapes for implementation of graphite ink

3.4.3. Experimental Analysis of Piezoresistive Material

Optimization of dimensions of piezoresistive layer is necessary to increase the sensitivity of the sensor. Based on aforementioned equations, calculations for optimization are completed and explained in the previous section. The experimental results, however, does not always match with the theoretical results. Therefore, an experiment is undertaken to verify the expected results for which twelve cantilever with a straight conductive line are produced.

Afterwards, the chosen five cantilevers are tested. The different level of change in their resistance values, which is due to their different width and length, are shown in the Figure 3.11. The graph shows that not only lengthening the piezoresistive but also narrowing its width increases the sensitivity of sensor.
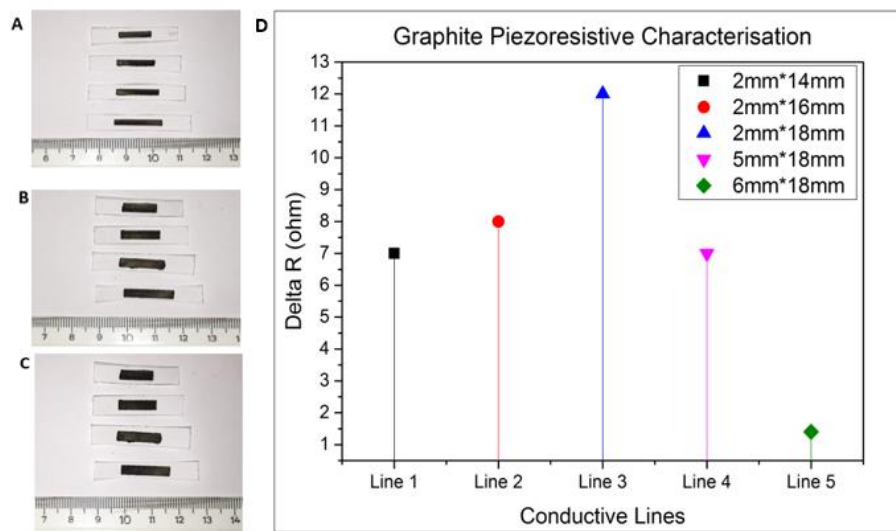

Figure 3.11. Conductive lines are produced by using graphite ink (A) 2mm width, 18,16,14 and 12 mm length respectively. (B) 5mm width, 18,16,14 and 12 mm length respectively. (C) 6mm width, 18,16,14 and 12 mm length respectively. (D) Conductive lines' resistance change are tested under same force (5mN)

Unfortunately, it is not possible to use straight conductive lines in the weight sensor because each tip of the piezoresistive line must be connected to the Wheatstone bridge circuit. Thus, a structure with two legs is required as mentioned. Therefore, three different designs are tested which are shown in Figure 3.12 These designs are prepared with various dimensions, as it is seen as in Figure 3.10, to see the impact of the shape.
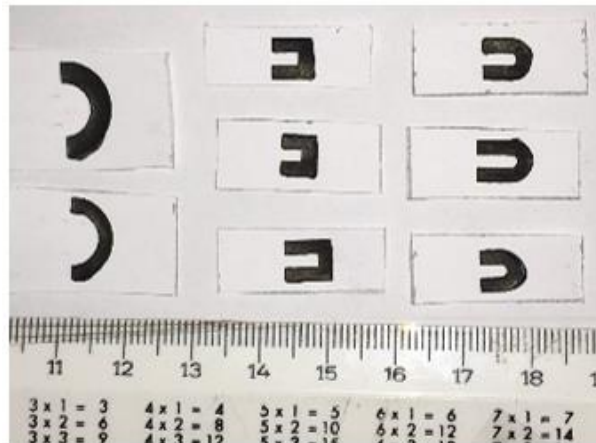
Figure 3.12. Piezoresistance shapes with different length and width

To begin with, the Shape 1 design in Figure 3.13 (A) is tested since it is the most common design according to the literature survey. The width of the resistor in that design is 2 mm whereas the lengths are chosen 6, 5, 7 mm respectively. The test result indicates that the length of this design impacts the sensitivity of sensor in the same way as the length of straight line does. The longer the resistor, the more the change in resistance increases.
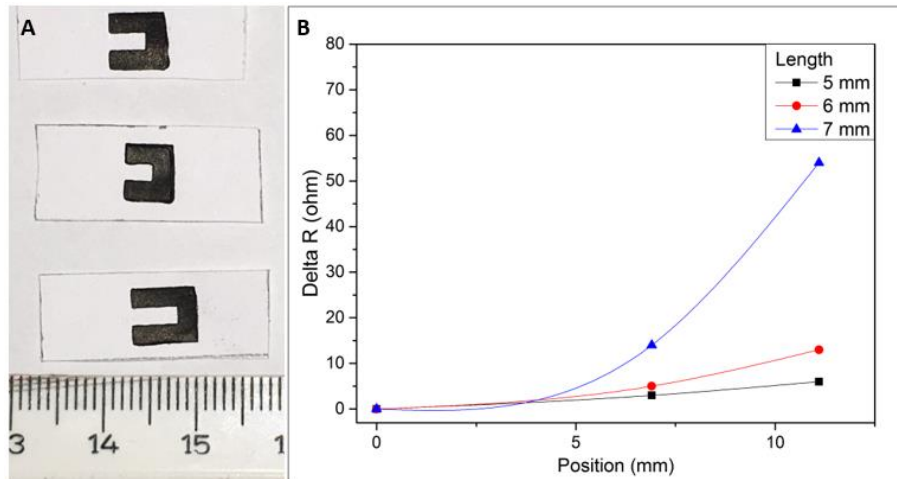
Figure 3.13. The length effect of piezoresistors in resistance change.

Afterwards, one sample from each design (Shape 1, Shape 2 and Shape 3) is tested. All of the selected samples have equal length and width, which are 7mm and 2mm respectively. Therefore, the independent variable of the experiment is the shapes of the designs, rather than the dimensions. The results of change in resistance are given in Figure 3.14. According to these results, the shape 1 design, which increases the change in resistance more than other designs, is the best choice.
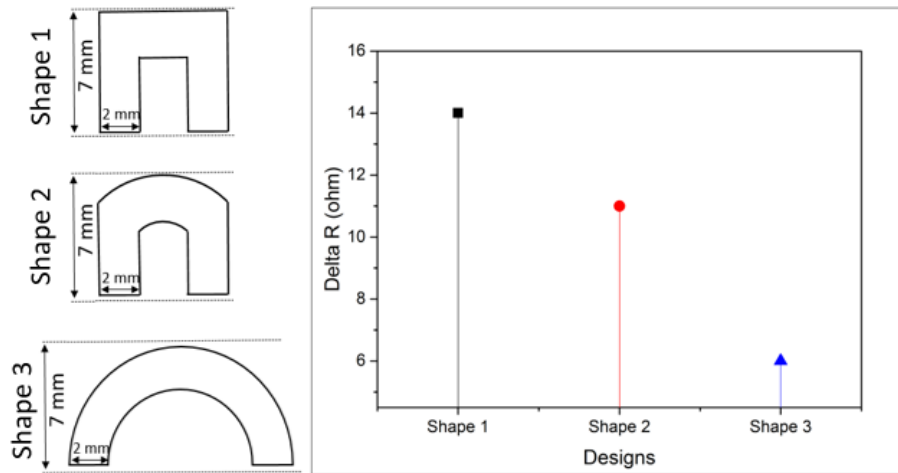
Figure 3.14. Different designs for implementation of graphite ink.

Based on all the tests and calculations conducted to define the behavior of the piezoresistive material, graphite for this thesis, it should be implemented with a width ranging from 1,65 to 2,2 and with a length ranging from 5,9 to 7,12.

The range of width is determined in accordance with the dimensions of the cantilever because the piezoresistive layer having U-shaped design must fit into the cantilever. Hence, the width of layer should be around 1/3 of the width of the cantilever. It enables to leave a vacancy between two legs and hence, enables to tolerate possible manufacturing errors.

The range of length, on the other hand, is depended on the theoretical explanations made before. The upper limit should be 1/5 of the length of the cantilever so that the length of piezoresistive layer can be negligible and enables us to use the Equation 3.6 in calculations. The lower limit should be around 1/6 of the length of the cantilever because the further decrease in its length cause an increase in its width due to their inverse relation, which is not desirable.
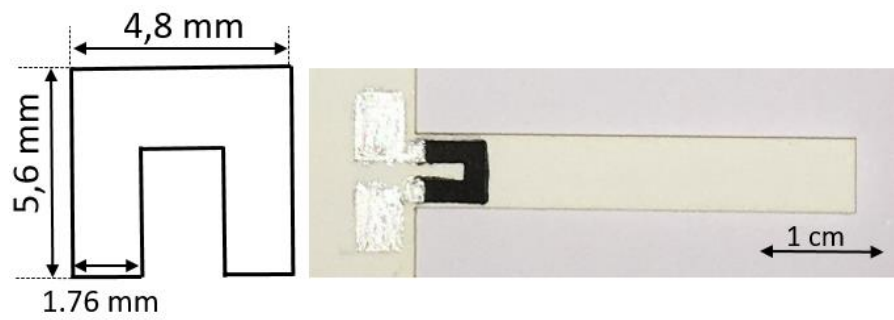
Figure 3.15. Implemented Graphite Ink

Consequently, the dimensions of the piezoresistive layer is determined as length being 5,6 mm and width being 1,76 mm as shown in Figure 3.15.

4. IMPLEMENTATION METHODS

4.1. ADDITIONAL PARTS

4.1.1. Borders and Alignment Platform

In production process of the weight sensor, aligning the stencils and the paper based cantilever is an important step. Since the piezoresistance is small, alignment is not easily achieved. It is also because of the cantilever's material which can be easily damaged. This damage can result in a loss of reliability. In order to avoid the difficulty of alignment and the possible damage, some additional paper is put aiming to create borders around the cantilever and stencil. The borders enabled to hold the structure without damaging it. It also makes the alignment step easier since it forms a larger area. The borders are taken out by scissors after the production of weight sensor.
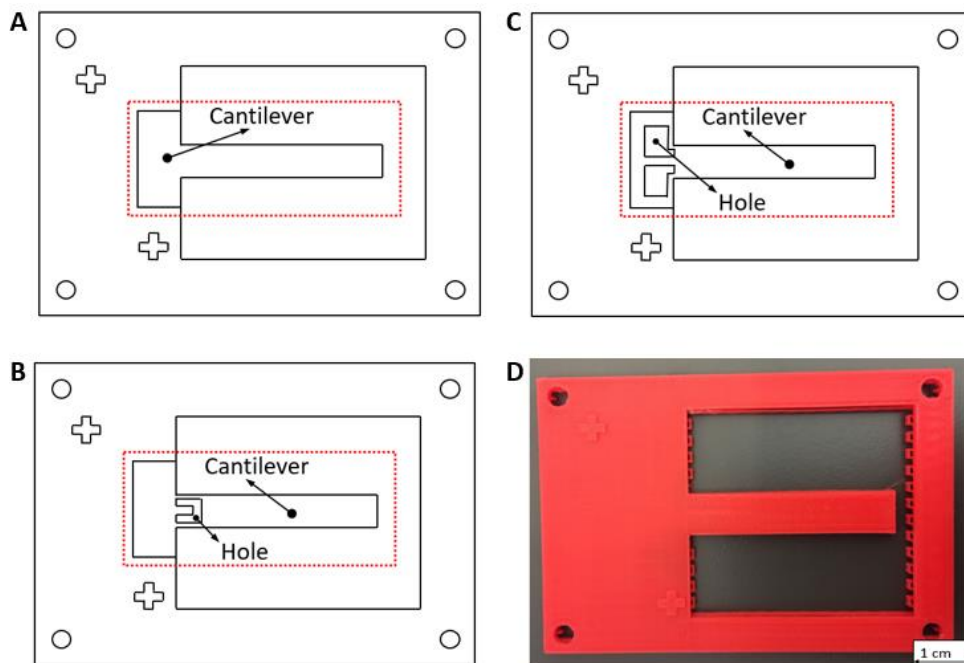
Figure 4.1. Additional Parts for Alignment and Fastening (A)Cantilever based with borders (B)Graphite stencil (C)Silver stencil (D)Alignment platform

As a separate step, it is necessary to produce an alignment and fastening platform to use in the fabrication process of weight sensor. As seen in Figure 4.1 D, the alignment platform is a 3D printed platform which is produced with PLA (Poli Lactic acid). It is a rectangular platform with an empty square inside which itself has a rectangular part in the middle to support structure. Around the rectangular part there is 1 mm upland. The platform has further four circular holes and two plus-shaped bulges.

As it is seen in Figure 4.1, some plus-shaped and circular holes are reamed on the border as well. By the help of these holes, the alignment step can be undertaken easily. When the holes overlap with the bulges on the alignment platform, then it means the structures are aligned. Then they can safely be fixed with screws. The structures can be aligned without the help of the holes as well, but there may be a deflection which is not tolerable regarding the sensitivity.
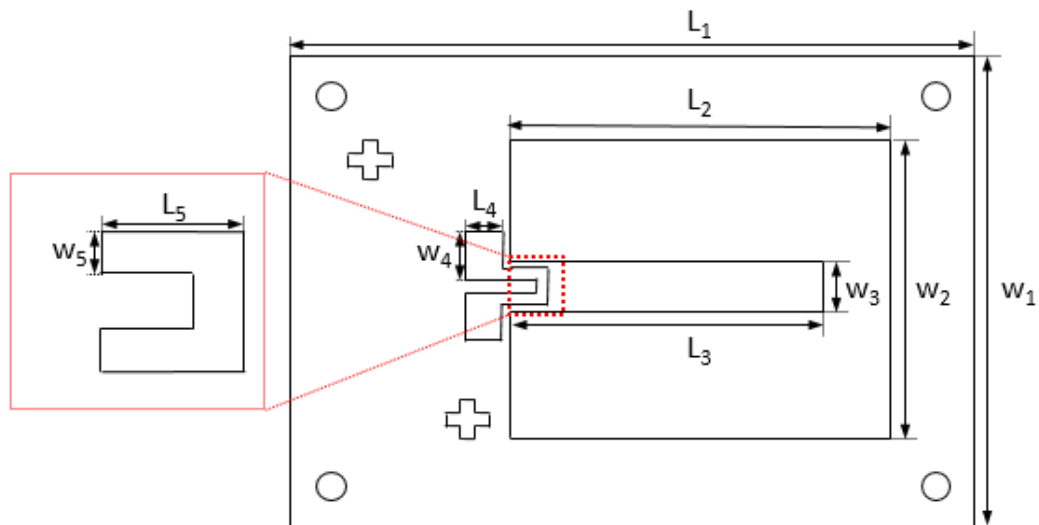
Figure 4.2. Drawing of Sensor (Dimensions are given in Table 2.6)

As a consequence, theoretical calculations and experimental results are analyzed together to decide the optimal dimensions of cantilever, graphite resistor and silver contact pad as seen in Figure 4.2. Additionally, the borders, circles and plus shapes are added to make the fabrication steps easier and to decrease the hand made errors. The values of the optimized dimensions are given in Table 4.1.

Table 4.1. Dimensions of Cantilever, Graphite Resistor and Silver Contact Pad

	w_1	w_2	w_3	w_4	w_5	L_1	L_2	L_3	L_4	L_5
Dimensions (mm)	50	50	66	2	1,76	91	50	35,6	2	5,6

4.1.2. Cantilever Base and Stencils

As it is explained in Section 1.3, the cantilever is composed of three main elements: paper base, graphite piezoresistive layer, and silver contact pad.

In Section 2, the design of the cantilever is decided in such a way that its dimensions are optimized to make sensitivity and accuracy maximum. Moreover, as explained in the section 4.1.1, the borders are also needed in order to make alignment and fastening easier. Technical drawings for cantilevers are made based on these optimal dimensions and these borders. The cantilevers are produced in accordance with the technical drawings and in their production process, Bristol paper is used which has 400µm thickness, 280 g/m^3 weight and 700kg/m^3 density. Young's modulus of Bristol paper is 2,52 GPa [75]. The Bristol paper is cut by laser cutter in accordance with the drawings.

Unlike cantilevers, the piezoresistive layer and contact pad requires the production of stencils. In Section 3, the design of the stencil for piezoresistive layer is decided in such a way that its dimensions are optimized to make sensitivity maximum. Moreover, as explained in Section 4.1.1, the borders are also needed in order to make alignment and fastening easier. Technical drawings for graphite stencils are made based on these optimal dimensions and these borders. The stencils are produced in accordance with the technical drawings and in their production process, photocopy paper is used. Young's modulus of this paper is 1.98 GPa (Canson Photocopy paper, 0.98kg/m^3).

The other type of stencils used in the project is for silver contact pad and those are also produced with photocopy paper. Differently from the piezoresistive layer, the dimensions of silver contact pads are not needed to be optimized because the effect of the contact pad's dimensions on the weight sensor is negligible. Only two criteria are needed to be paid attention to. First, the pad should be wide enough to enable piezoresistive layer and the

Wheatstone bridge to connect. Second, it should be as small as possible to use the silver ink efficiently. Regarding these criteria, the dimensions of the contact pad are decided as both width and length being 2mm.

4.2. SCREEN PRINTING IMPLEMENTATION

The materials required in production process are paper based cantilever (Bristol Paper, 280 g/m^3), graphite ink (Bare Conductive Electric paint), silver ink (Circuit Scribe conductive ink pen) and two stencils (one for graphite piezoresistive layer and one for silver contact pad). The tools specially needed are alignment platform and PLA screws.
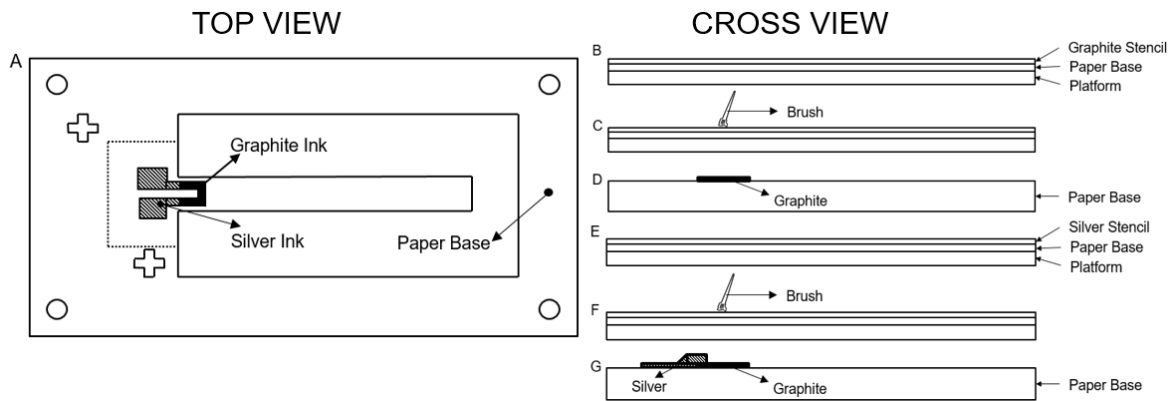
Figure 4.3. Fabrication steps of weight sensor

There are two main steps in production process:

Firstly, the graphite piezoresistive layer should be implemented with the following process. The cantilever is placed on the alignment platform. Then, the stencil is put on the cantilever and those two are aligned with the help of plus shapes on the alignment platform. Afterwards, the cantilever, the stencil and the alignment platform are fastened by PLA screws. Graphite ink is implemented on the cantilever by brush (Figure 4.3 C). Then, the alignment platform is taken out and the merged stencil and cantilever is baked for twenty minutes on 60 ^{o}C hot plate. After baking, the cantilever and stencil are separated.

Second step of fabrication is the implementation of silver ink with the following the similar process. The stencil is aligned with the cantilever produced in the first step on the alignment

platform. Then, those three are fastened by PLA screws. Afterwards, silver ink is applied by brush (Figure 4.3 F). After one or two minutes, the silver ink dries and becomes ready to be separated. So, the alignment platform is taken out and the cantilever and the stencil are separated. This is how the cantilever with graphite which is produced in the first step also has a silver layer and the end result cantilever is shown in Figure 4.3 (A). The additional paper borders are cut off and the remaining part is the weight sensor.

5. RESULTS AND DISCUSSION

5.1. TEST SETUP

In this project, two different test setups are prepared. First one is for weight sensor and the second one is for the weight sensor with magnetic amplifier whose difference is the addition of a magnet.

As seen in Figure 5.1, a wooden holder is put to increase the weight sensor's ground clearance. The weight sensor is located on the top of the holder and it is connected to the Wheatstone bridge circuit by its silver contact pad. Wheatstone bridge circuit is also connected to a power supply and to a digital multimeter. In this setup, the digital multimeter is used to measure output voltage of the Wheatstone bridge circuit. Moreover, a weight plate, a place to put the weights that are to be measured, is tied by a rope to the free end of the cantilever.

In the first setup, there is not any magnet in the test setup and hence, the output is only related to the weight. In the second system, however, the magnet is located under the weight plate in a way it touches the plate. The magnet is pulled downwards which pulls the plate as well. However, at a certain point, the connection between those two is broken meaning that the magnet still being pulled downwards can no longer cause the plate to go downwards. Right before that breaking point, the voltage reaches its peak and the peak value of voltage is written down as the output for this weight. The test is repeated with distinct weights that are to be measured.
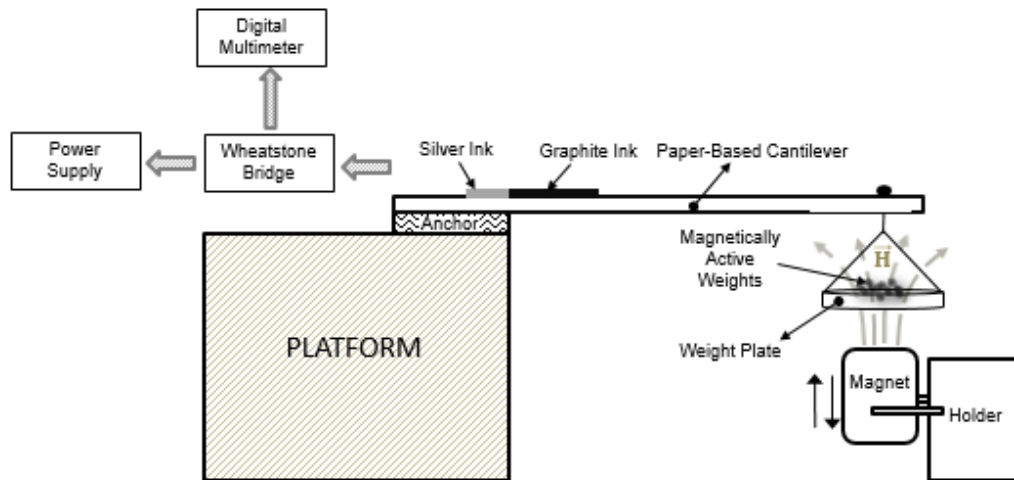
Figure 5.1. Schematic of Test Setup for Weight Sensor with Magnetic Amplifier.

5.2. TEST RESULTS

The main purpose of the weight test is to   observe the weight sensor behavior which is reflected in the change faced by voltage value and/or in the displacement.

In the first setup, which is the one without magnetic amplifier, in order to observe the relation between the weights and the voltage, a drop of pure water is used as weight. Water's density is approximately $1g/cm^3$. Drops are added with pipette leading an increase in the weight measured. The evaporation is neglected. The relation can be seen in Figure 5.2, which indicates that the weights can be measured with 20 mg resolution by this weight sensor.
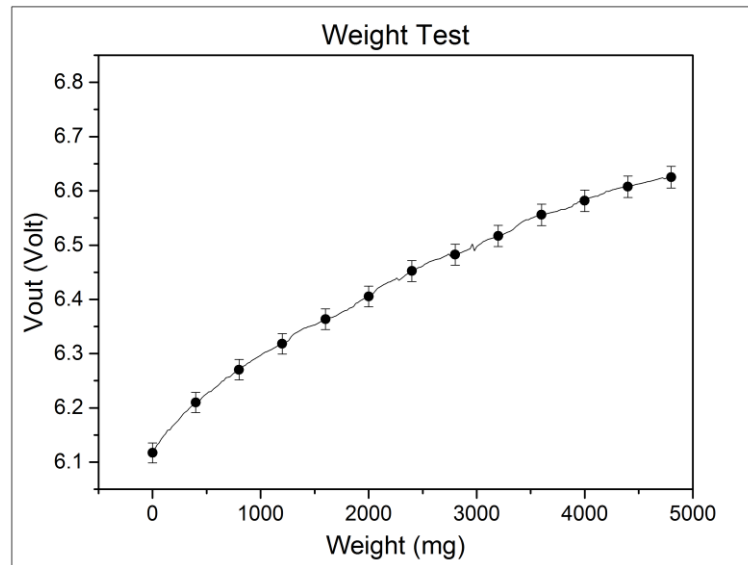
Figure 5.2. Weight Test correspond to Voltage and Weight Relation[1]

The reverse test is conducted to see whether the change in the voltage value follows the exact same line when the weight is declined. By using the pipette, the water is collected and the weight is reduced step by step. The vaporization during the test is ignored. The result indicates that the lines for increasing weights (loading) and decreasing weights (unloading) do not overlap which indicates the existence of hysteresis due to the paper deformation. In Figure 5.3, the lines showing both relations are given.

---

[1] In the graph, one of the every twenty step is shown.
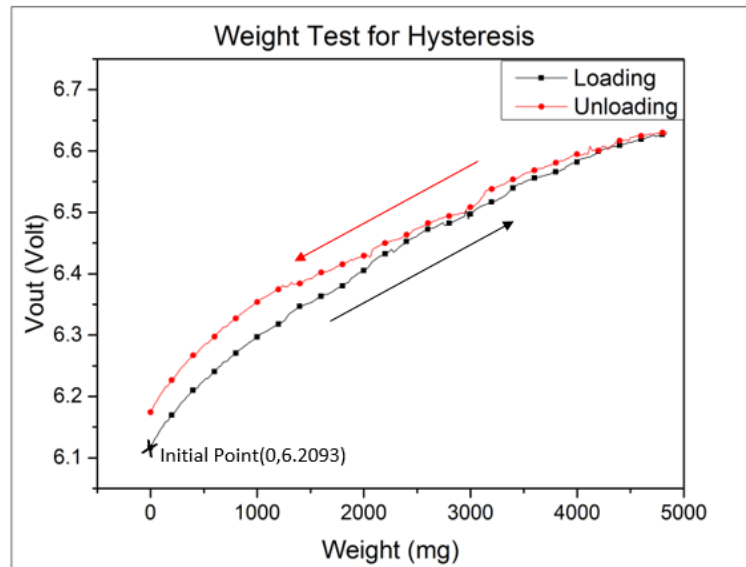
Figure 5.3. Weight Test for Observing Deformation[2]

The other factor determining the sensor behavior is reflected in the displacement amount. The test is conducted to observe the relation between the weights and the displacement amounts. The test is both conducted for increasing weights (loading) and reversely for decreasing weights(unloading). Displacement amounts for both are measured by using Image J Software, which is an image processing program. For each weight, photos of cantilever's stance are taken and the displacement amounts are measured accordingly. The results are shown in Figure 5.4.

---

[2] In the graph, one of the every ten step is shown.
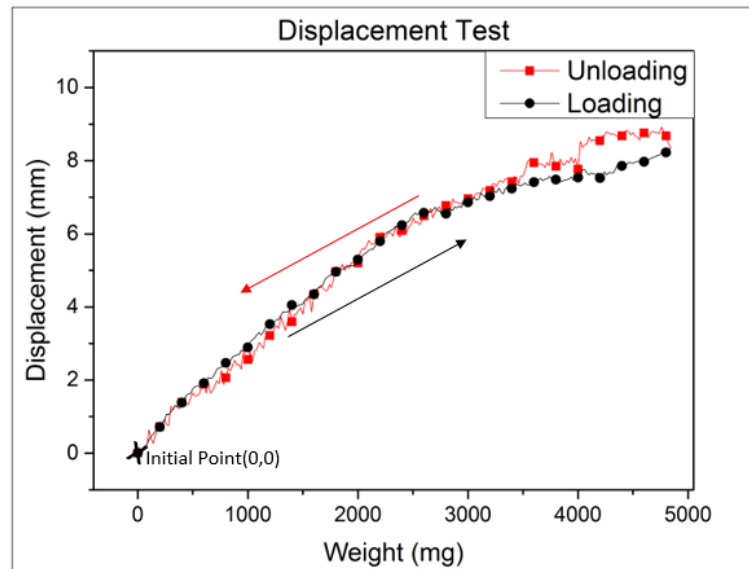
Figure 5.4. Displacement Test for both Loading and Unloading[3]

In the second setup, which is the one with the magnetic amplifier, water cannot be used as the weight because it is not a matter magnetically active. Therefore, in this setup, the particles made of wire magnetically active are used as the weights. The relation between the weights and the voltage value is observed and can be seen in Figure 5.5.
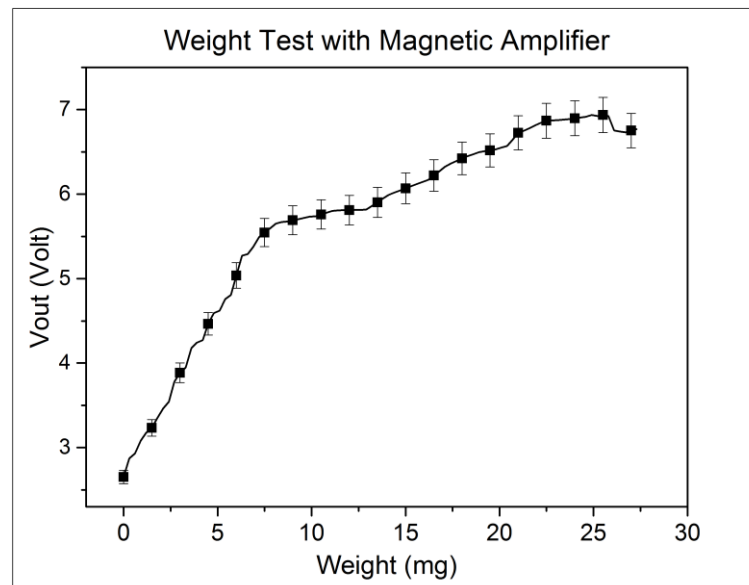
Figure 5.5. Weight Test with Magnetically Amplified Sensor[4]

---

[3] One of every ten step is shown in the graph.
[4] In the graph, one of the every five step is shown.

The curve characteristic of the plot in Figure 5.5 illustrates that over 8 mg weight, this sensor should not be used since its response is changed. In this sensor, the range of the system is 0.3 mg to 8 mg.

5.3. DISCUSSION

Two setups produced in the thesis are to form two different weight sensor devices. The first device is similar to the existing ones in the literature. The weights can be measured by this device with 20 mg resolution and 0 to 2.5 g range. Based on the test results indicating the existence of hysteresis, the sensor can only be used once and just for loading. Due to paper deformation, the same sensor cannot be used in unloading process as well.

When the plots in Figure 5.3 and 5.4 are compared, the hysteresis in the output voltage is caused by the damage of the piezoresistor. It is because the loading curves in Figure 5.4 is close to unloading curve, on the other hand, the loading curve and unloading curve in Figure 5.3 is much more separated from each other. In Figure 5.6, it is noticed that the change observed in the read-out circuit is not as much as the changed observed in displacement. Although the lower responsiveness of read-out circuit seems like a disadvantage, it actually creates an advantage by enabling small changes in displacement to be ignored, such as vibrations which are generated on the free end of the cantilever as a result of error of the tests. It prevents the vibrations from impacting the output voltage and hence, the sensor acts as low pass filter.
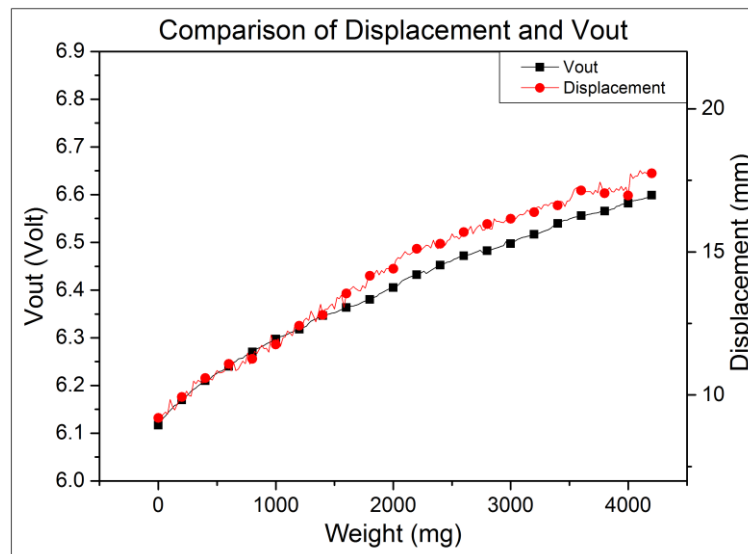
Figure 5.6. Weight Test to Observe Displacement and Voltage Change Relation[5]

The second device, on the other hand, is distinct from the already existing ones since it includes a magnetic amplifier. The inclusion of a magnet in the device yields a significant difference since the weight measured ends up having higher effective mass in the second device. The higher effective mass yield higher values of sensitivity (0.4V/mg instead of 0.035mV/mg). The gain of the second device is approximately 11700 compare to the first one. This gain has the utmost importance because sensitivity is the most significant parameter in the weight sensor device which are to be used to detect the biological and chemical particles. Therefore, the magnetic amplifier is beneficial as it has an increasing impact on the sensitivity.

Two points must be stated regarding the comparison of the two devices. First, it is possible to determine the weights with higher frequency by the second device than by the first device. The matching weights of two devices for the same value of change in output voltage can be seen in Figure 5.8. The reference points of comparison graph are marked in Figure 5.7. The second point is that the range of the second device (0-7.6mg) is narrower than the first device (0-2.5g).

Furthermore, when the Figure 5.8 on the comparison of two devices is examined, a prominent point is recognized. The test is conducted with 0.3 mg weights because there is

---

[5] In the graph, bullets are located for one of every ten steps.

not any lighter weight available; but the resolution steps can safely be assumed as 176 times more frequent (1.7 µg). It is mainly because the gain of the second device is approximately 11700 in comparison with first device.
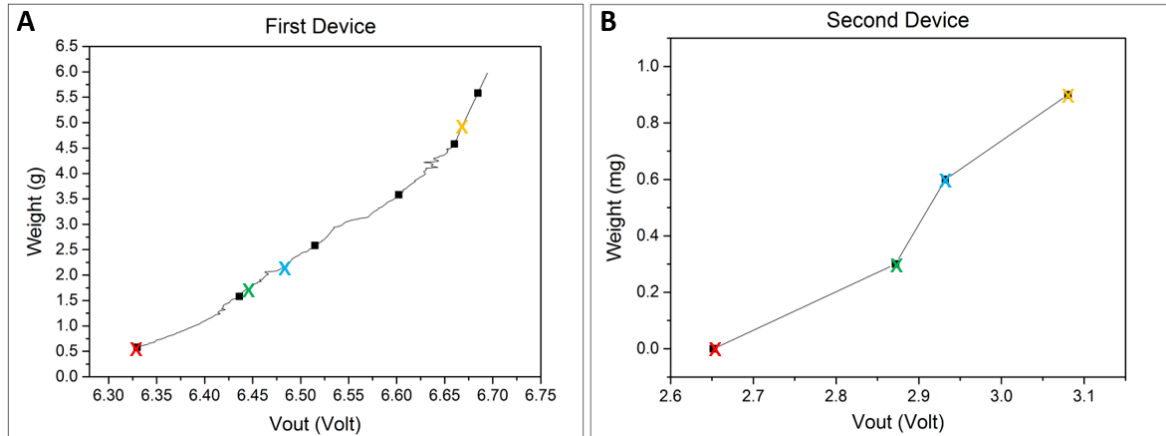
Figure 5.7. Weight and Change in Output Voltage Graph for Both Devices

Moreover, in Figure 5.6, the results show that in both sensor types, the change in the voltage and in the displacement are directly proportional. Therefore, it is safe to state that there is a direct proportion between the output voltage, resistance change, displacement of cantilever, bending angle and applied force.
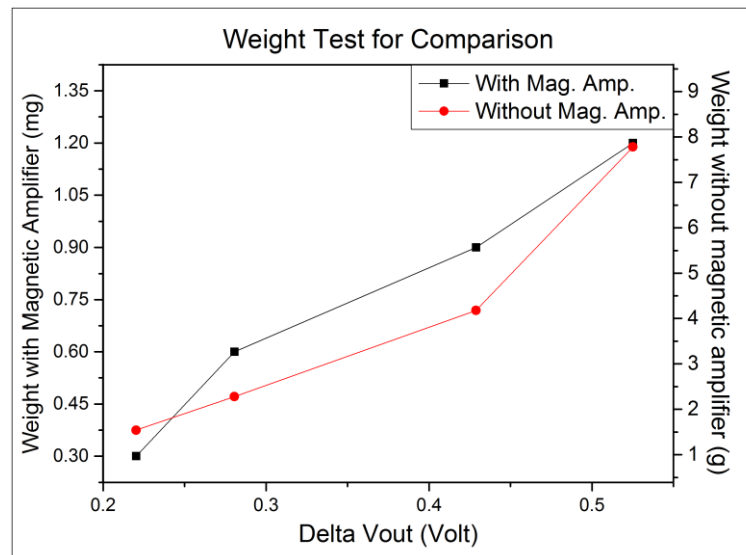

Figure 5.8. Comparison of Weight Sensors

6. SUMMARY AND CONCLUSION

In this thesis, we manage to produce two weight sensor devices. The sensing unit of both is produced from the Bristol paper with 400µm thickness which is cut as a shape of cantilever with 6.16 width and 35.6 mm length by laser cutter. Then, they are coated by piezoresistive material and silver ink. After the implementation, two setups as a weight sensor device are set. In the setups, there are read-out circuit, sensing unit and weight plate. In the second setup, there is an additional magnetic amplifier which improves the sensitivity of the system since it amplifies the effective mass of each weights. The devices and a well-known piezoresistive pressure sensor is compared and their properties are given in Table 6.1.

Table 6.1. Comparison table of weight sensors

	Pressure Sensor [37]	First Device	Second Device
Dynamic Range	0-15g	0-2.5g	0-7,6mg
Resolution	25mg	20mg	1.7 µg (assumed)
Gain in Resolution	1	1,25	14706
Sensitivity	8.24mV/g	0.035mV/mg	0.4V/mg
Gain in Sensitivity	1	4.25	48543
Commercial Price per Test	0,04$	0,28$	0,28$
Commercial Price of Device	-	20$	30$
Biological/Chemical Particle Detection	Not Possible	Not Possible	Possible (0.03 M solution)
Measurable Particle Type	Magnetically Active/Inactive Particles	Magnetically Active/Inactive Particles	Magnetically Active Particles

A prominent point takes attention in Table 6.1. Although the first devices sensitivity is approximately four times higher than the pressure sensor, the gain in resolution is worser. It is because the detectable voltage change in read-out circuit is 0.7 mV. Additionally, first device can measure the weights with 20 mg resolution whereas the second one can measure with 1.7 µg resolution based on the assumption. Accordingly, the second one is chosen to be used to detect biological or chemical particles. The biosensor, which is modified from the

second device, is assumed to measure 0 to 136 M solution with 0.03 M resolution. However, it is important to mention that even the second sensor's sensitivity can be improved in future studies by an additional instrumental amplifier connected to the Wheatstone Bridge Circuit. The instrumental amplifier can theoretically improve the sensitivity of sensor 100 times. In addition to this, in order to accelerate the fabrication process of the weight sensor, two printers are modified and can be used in future studies.

REFERENCES

[1]   M. Rouse, "Sensor," 2012. [Online]. Available: http://whatis.techtarget.com/definition/sensor.

[2]   C. Lui, Foundation of MEMS, United State: Pearson Education, 2012.

[3]   W. Ye, S. Mukherjee and N. C. MacDonald, "Optimal Shape Design of an Electrostatic Comb Drive in Microelectromechanical Systems," *Journal of Microelectromechanical System,* vol. 7, no. 1, pp. 16-26, 1998.

[4]   M. Sakata, Y. Komura, T. Seki, K. Kobayashi, K. Sano and S. Horüke, "Micromachined Relay which Utilizes Single Crystal Silicon Electrostatic Actuator," *IEEE,* pp. 21-24, 1999.

[5]   V. Milanovic, M. Gaitan, E. D. Bowen, N. H. Tea and M. E. Zaghloul, "Thermoelectric Power Sensor for Microwave Applications by Commercial CMOS Fabrication," *IEEE Electron Device Letters,* vol. 18, no. 9, pp. 450-452, 1997.

[6]   M. J. Sinclair, "A High Force Low Area MEMS Thermal Actuator," in *IEEE Intersociety Conference on Thermal Phenomena*, Washington DC, 2000.

[7]   C. R. Thomas, D. P. Ferris, J.-H. Lee, E. Choi, M. H. Cho, E. S. Kim, J. F. Stoddart, J.-S. Shin, J. Cheon and J. I. Zink, "Noninvasive Remote-Controlled Release of Drug Molecules in Vitro Using Magnetic Actuation of Mechanized Nanoparticles," *American Chemical Society,* vol. 132, pp. 10623-10625, 2010.

[8]   C.-S. Park, J. Park and D.-W. Lee, "A Piezoresistive Tactile Sensor Based on Carbon Fibers and Polymer Substrates," *Microelectronic Engineering,* vol. 86, pp. 1250-1253, 2009.

[9]   Y.-H. Wang, C.-Y. Lee and C.-M. Chiang, "A MEMS-Based Air Flow Sensor with a Free-standing Micro-Cantilever Structure," *Sensors,* vol. 7, pp. 2389-2401, 2007.

[10]   H. J. M. T. A. Adriaens, W. L. de Koning and R. Banning, "Modeling Piezoelectric Actuators," *ASME Transactions on Mechatronics,* vol. 5, no. 4, pp. 331-341, 2000.

[11]   C. Xu, S. Wang, G. Tang, D. Yang and B. Zhou, "Sensing Characteristics of Electrostatic Inductive Sensor for Flow Parameters Measurement of Pneumatically Conveyed Particles," *Journal of Electrostatics,* vol. 65, pp. 582-592, 2007.

[12] J. Ma and Y. Yan, "Design and Evaluation of Electrostatic Sensors for the Measurement of Velocity of Pneumatically Conveyed Solids," *Flow Measurement and Instrumentation,* vol. 11, pp. 195-204, 2000.

[13] J. I. Seeger and B. E. Boser, "Dynamics and Control of Parallel-Plate Actuators beyond the Electrostatic Instability," in *International Conference on Solid-State Sensors and Actuators*, Sendai, 1999.

[14] G. J. Fitzgerald, D. Rodriguez, L. K. Christensen, R. Belford, V. O. Sadras and T. R. Clarke, "Spectral and Thermal Sensing for Nitrogen and Water Status in Rainfed and Irrigated Wheat Environments," *Precision Agric,* vol. 7, pp. 233-248, 2006.

[15] J. Mora, A. Diez, J. L. Cruz and M. V. Andres, "A Magnetostrictive Sensor Interrogated by Fiber Gratings for DC-Current and Temperature Discrimination," *IEEE Photonics Technology Letters,* vol. 12, no. 12, pp. 1680-1682, 2000.

[16] A. Jain, H. Qu, S. Todd and H. Xie, "A Thermal Bimorph Micromirror with Large Bi-Directional and Vertical Actuation," *Sensors and Actuators: Physics,* vol. 122, pp. 9-15, 2005.

[17] V. Leonov, T. Torfs, P. Fiorini and C. V. Hoof, "Thermoelectric Converters of Human Warmth for Self-Powered Wireless Sensor Nodes," *IEEE Sensors Journal,* vol. 7, no. 5, pp. 650-657, 2007.

[18] "Electronics Hub," Electronicshub.org, 2017. [Online]. Available: http://www.electronicshub.org/?s=thermocouple.

[19] S. C. Minne, S. R. Manalis and C. F. Quate, "Parallel Atomic Force Microscopy Using Cantilevers with Integrated Piezoresistive Sensors and Integrated Piezoelectric Actuators," *American Institude of Physics,* vol. 67, no. 26, pp. 3918-3920, 1995.

[20] N. Yazdi, F. Ayazi and K. Najafi, "Micromachined Inertial Sensors," *IEEE,* vol. 88, no. 8, pp. 1640-1659, 1998.

[21] L. Lin, H.-C. Chu and Y.-W. Lu, "A Simulation Program for the Sensitivity and Linearity of Piezoresistive Pressure Sensors," *Microelectromechanical Systems,* vol. 8, no. 4, pp. 514-522, 1999.

[22] J. Sirohi and I. Chopra, "Fundamental Understanding of Piezoelectric Strain Sensors," *Intelligent Material Systems and Structures ,* vol. 11, pp. 246-257, 2000.

[23] M. Avila, M. Zougagh, A. Escarpa and A. Rios, "Supported Liquid Membrane-Modified Piezoelectric Flow Sensor with Molecularly Imprinted Polymer for the Determination of Vanillin in Food Samples," *Talanta,* vol. 72, pp. 1362-1369, 2007.

[24] J. Dargahi, M. Parameswaran and S. Payandeh, "A Micromachined Piezoelectric Tactile Sensor for an Endoscopic Grasper—Theory, Fabrication and Experiments," *Microelectromechanical Systems,* vol. 9, no. 3, pp. 329-335, 2000.

[25] H. Shintaku, T. Nakagawa, D. Kitagawa, H. Tanujaya, S. Kawano and J. Ito, "Development of Piezoelectric Acoustic Sensor with Frequency Selectivity for Artificial Cochlea," *Sensors and Actuators A: Physical,* vol. 158, pp. 183-192, 2010.

[26] G. Caruso, S. Galeani and L. Menini, "Active Vibration Control of an Elastic Plate using Multiple Piezoelectric Sensors and Actuators," *Simulation Moselling Practice and Theory,* vol. 11, pp. 403-419, 2003.

[27] U. Wafer, "AZO Nano," AZONetwork, 2014. [Online]. Available: http://www.azonano.com/article.aspx?ArticleID=3835.

[28] Y. Li, "Biosensors," in *CIGR Handbook of Agricultural Engineering Volume VI Information Technology*, Michigan, USA, American Society of Agricultural Engineers, 2006, pp. 52-93.

[29] J. Comer, "Semiquantitative Specific Test Paper for Glucose in Urine," *Analytical Chemistry,* pp. 1748-1750, 1956.

[30] C. Cheng, A. Martinez, J. Gong, C. Mace, S. Phillips, E. Carrilho, K. Mirica and G. Whitesides, "Paper-Based ELISA," *Angewandte Chemie,* vol. 122, pp. 4881-4884, 2010.

[31] "Wikipedia The Free Encyclopedia," Wikipedia Foundation Inc., 2013. [Online]. Available: https://tr.wikipedia.org/wiki/ELISA.

[32] K. Dhaval and E. Mehul, "21st Century's Revolution: MEMS Technology," 2014. [Online]. Available: https://www.slideshare.net/DhavalKaneria/dhaval-ieee-final.

[33] R. V. Martinez, C. R. Fish, X. Chen and G. M. Whitesides, "Elastromaric Origami: Programmable PAper-Elastomer Composites as Pheumatic Actuators," *Advance Function Material,* vol. 22, pp. 1376-1384, 2012.

[34] M. M. Hamedi, V. E. Campbell, P. Rothemund, F. Güder, D. C. Christodouleas, J.-F. Bloch and G. M. Whitesides, "Electrically Activated Paper Actuators," *Advance Function Material,* vol. 26, pp. 2446-2453, 2016.

[35] Z. Nie, C. A. Nijhuis, J. Gong, X. Chen, A. Kumachev, A. W. Martinez, M. Narovlyansky and G. M. Whitesides, "Electrochemical Sensing in Paper-Based Microfluidic Devices," *Lab on a Chip,* vol. 10, pp. 477-483, 2009.

[36] A. D. Mazzeo, W. B. Kalb, L. Chan, M. G. Killian, J.-F. Bloch, B. A. Mazzeo and G. M. Whitesides, "Paper-Based Capacitive Touch Pads," *Advance Material,* vol. 24, pp. 2850-2856, 2012.

[37] X. Liu, M. Mwangi, X. Li and G. Whitesides, "Paper-Based Piezoresistive MEMS Force Sensors," *Lab Chip,* vol. 11, no. 13, pp. 2189-2196, 2012.

[38] T. Ren, H. Tian, D. Xie and Y. Yang, "Flexible Graphite-on-Paper Piezoresistive Sensors," *Sensors,* pp. 6685-6694, 2012.

[39] K. Crowley, D. Nakidde, J. Travis and M. Agah, "Paper-Based MEMS Hair Cell Array," *Sensors,* pp. 1-4, 2013.

[40] A. Bessonova, M. Kirikova, S. Haque, I. Gartseev and M. Bailey, "Highly Reproducible Printable Graphite Strain Gauges for Flexible Devices," *Sensors and Actuators A: Physical,* vol. 206, pp. 75-80, 2014.

[41] K. Cammann, "Bio-sensors Based on Ion-Selective Electrodes," *Fresenius' Zeitschrift für Analytische Chemie,* vol. 287, no. 1, pp. 1-9, 1977.

[42] N. Arora, "Science Being," 2013. [Online]. Available: http://www.sciencebeing.com/2013/10/biosensors-history/.

[43] B. Dogan, "Dersler," İTU, 2014. [Online]. Available: web.itu.edu.tr/~bdogan/dersler/bioay1314/kimyasal_donus.doc.

[44] S. Mohanty and E. Kougianos, "Biosensor: A Tutorial Review," *Biosensor: A Tutorial Review,* pp. 35-40, 2006.

[45] U. Kökbaş, L. Kayrın and A. Tuli, "Biyosensörler ve Tıpta Kullanım Alanları," *Biyosensörler ve Tıpta Kullanım Alanları,* pp. 499-513, 2013.

[46] M. Pohanka and P. Skladal, "Electrochemical Biosensors-Principles and Applications," *Journal of Applied Biomedicine,* pp. 57-64, 2008.

[47] Y. Li, W. Roy, P. Vereecken and L. Lagae, "An ELISA-Based Amperometric Biosensor within a Photo-Patternable Adhesive Microfluidic Channel," in *IEEE-NEMS*, Xi'an China, 2015.

[48] T. Kawashima and G. Rechnitz, "Potentiometric Enzyme Electrode for Uric Acid," *Analytica Chimica Acta.,* vol. 83, pp. 9-17, 1976.

[49] A. Tarasova, D. Gray, M. Tsai, N. Shields, A. Montrose, N. Creedon, P. Lovera, A. O'Riordan, M. Mooney and E. Vogel, "A Potentiometric Biosensor for Rapid on-site Disease Diagnostics," *Biosensors and Bioelectronics,* vol. 79, pp. 669-678, 2016.

[50] A. Stobiecka, H. Radecka and J. Radecki, "Novel Voltammetric Biosensor for Determining Acrylamide in Food Samples," *Biosensors and Bioelectronics,* vol. 22, no. 9-10, pp. 2165-2170, 2007.

[51] N. Reta, A. Michelmore, C. Saint, B. Prieto-Simón and N. Voelcker, "Porous Silicon Membrane-Modified Electrodes for Label-Free Voltammetric Detection of MS2 Bacteriophage," *Biosensors and Bioelectronics,* vol. 80, pp. 47-53, 2016.

[52] A. Mars, C. Parolo, A. Escosura-Muniz, N. Raouafi and A. Merkoçi, "Control of Electron-Transfer in Immunonanosensors by Using Polyclonal and Monoclonal Antibodies," *Electroanalysis,* vol. 28, pp. 1795-1802, 2016.

[53] C. Chouteaua, S. Dzyadevychc, C. Durrieua and J. Chovelon, "A Bi-Enzymatic Whole Cell Conductometric Biosensor for Heavy Metal Ions and Pesticides Detection in Water Samples," *Biosensors and Bioelectronics,* vol. 21, no. 2, pp. 273-281, 2005.

[54] K. Jaruwongrungsee, U. Waiwijit, A. Wisitsoraat, M. Sangworasil, C. Pintavirooj and A. Tuantranont, "Real-Time Multianalyte Biosensors Based on Interference-Free Multichannel Monolithic Quartz Crystal Microbalance," *Biosensors and Bioelectronics,* vol. 67, pp. 576-581, 2015.

[55] K. Buchapudi, X. Huang, A. Yang, H. Ji and T. Thundat, "Microcantilever Biosensors for Chemicals and Bioorganisms," *Analyst,* vol. 136, no. 8, pp. 1539-1556, 2011.

[56] M. Yakovlevaa, S. Bhandb and B. Danielssonc, "The Enzyme Thermistor—A Realistic Biosensor Concept. A Critical Review," *Analytica Chimica Acta,* vol. 766, pp. 1-12, 2013.

[57] T. Chan, M. Verma and F. Gu, "Optimization of Polydiacetylene-Coated Superparamagnetic Magnetite Biosensor for Colorimetric Detection of Biomarkers," *Journal of Nanoscience and Nanotechnology,* vol. 15, no. 4, pp. 2628-2633, 2015.

[58] K. Wee, G. Kang, J. Park, J. Kang, D. Yoon, J. Park and T. Kima, "Novel Electrical Detection of Label-Free Disease Marker Proteins using Piezoresistive Self-Sensing Micro-Cantilevers," *Biosensors and Bioelectronics,* vol. 20, pp. 1932-1938, 2005.

[59] R. Zhao, W. Ma, Y. Wen, J. Yang and X. Yu, "Trace Level Detections of Abrin with High SNR Piezoresistive Cantilever Biosensor," *Sensors and Actuators B: Chemical,* vol. 212, pp. 112-119, 2015.

[60] J. Tashkhouriana, M. Hormozi-Nezhadb, J. Khodaveisid and R. Dashtie, "A Novel Photometric Glucose Biosensor Based on Decolorizing of Silver Nanoparticles," *Sensors and Actuators B: Chemical,* vol. 158, no. 1, pp. 185-189, 2011.

[61] D. Sotnikov, N. Byzova, A. Zherdev, S. Eskendirova, K. Baltin, K. Mukanov, E. Ramankulov, E. Sadykhov and B. Dzantiev, "Express Immunochromatographic Detection of Antibodies against Brucella Abortus in Cattle Sera Based on Quantitative Photometric Registration and Modulated Cut-Off Level," *Journal of Immunoassay and Immunochemistry,* vol. 36, no. 1, pp. 80-90, 2015.

[62] Y. Huang, H. Yang and Y. Ai, "DNA Single-Base Mismatch Study Using Graphene Oxide Nanosheets-Based Fluorometric Biosensors," *Anal. Chem.,* vol. 87, no. 8, pp. 9132-9136, 2015.

[63] T. Shojaei, M. Salleh, K. Sijam, R. Rahim, A. Mohsenifar, R. Safarnejad and M. Tabatabaei, "Fluorometric Immunoassay for Detecting the Plant Virus Citrus Tristeza Using Carbon Nanoparticles Acting as Quenchers and Antibodies Labeled with CdTe Quantum Dots," *Microchimica Acta,* vol. 183, no. 7, pp. 2277-2287, 2016.

[64] D. Nivens, T. McKnight, S. Moser, S. Osbourn, M. Simpson and G. Sayler, "Bioluminescent Bioreporter Integrated Circuits: Potentially Small, Rugged and Inexpensive Whole-Cell Biosensors for Remote Environmental Monitoring," *Applied Microbiology,* vol. 96, no. 1, pp. 33-46, 2004.

[65] R. Art, I. Hartog, S. Zijlema, V. Thijssen, S. Van der Beelen and M. Merkx, "Detection of Antibodies in Blood Plasma Using Bioluminescent Sensor Proteins and a Smartphone," *Analitical Chemistry,* vol. 88, no. 8, pp. 4525-4532, 2016.

[66] J. Newman, L. Tigwell, P. Warner and A. Turner, "Biosensors: Boldly Going into the New Millennium," *Sensor Review,* vol. 21, pp. 268-271, 2001.

[67] Y. Liedberg, "Biosensors," in *CIGR Hanbook of AGricultural Engineering Volume VI Information Technology*, Michigan, American Society of AgriculturalEngineers, 2006.

[68] J. Yu, L. Ge, J. Huang, S. Wang and S. Ge, "Microfluidic Paper-Based Chemiluminescence Biosensor for Simultaneous Determination of Glocose and Uric Acid," *Lab Chip,* pp. 1286-1291, 2011.

[69] N. Opitz and D. Lübbers, "Optical Fluorescence Sensors for Continuous Measurement of Chemical Concentrations in Biological Systems," *Sensors and Actuators,* vol. 4, pp. 641-654, 1983.

[70] M. Aizawa, A. Morioka, H. Matsuoka, S. Suzuki, Y. Nagamura, R. Shinohara and I. Ishiguro, "An Enzyme Immunosensor for IgG," *Journal of Solid-Phase Biochemistry,* vol. 1, pp. 319-328, 1976.

[71] J. Plewa and J. Michael, "Mutagenicity of Atrazine: A Maize-Microbe Bioassay," *Mutation Research/Environmental Mutagenesis and Related Subjects,* vol. 38, no. 4, pp. 287-292, 1976.

[72] "Electrician Traning," Integrate Publishing Inc., 2016. [Online]. Available: http://electriciantraining.tpub.com/14193/css/Chapter-3-Quantitative-Measurements-89.htm.

[73] "Wikipedia The Free Encyclopedia," Wikipedia Foundation Inc., 2017. [Online]. Available: https://en.wikipedia.org/wiki/Carbon#Production.

[74] "chemhume," Chemhume Co., 2017. [Online]. Available: http://www.chemhume.co.uk/ASCHEM/Unit%201/Ch3IMF/Chemical%20Struct.htm.

[75] J. Tryding, IN-PLANE FRACTURE OF PAPER, Sweden: LUND Institute of Technology, 1996.

[76] J. Tryding, "Lunds Tekniska Högskola," 1996. [Online]. Available: http://www.lth.se/fileadmin/byggnadsmekanik/publications/tvsm1000/web1008.pdf.

[77] Maximous, "Print Conductive Circuits with an Inkjet Printer," Instructables, 2015. [Online]. Available: http://www.instructables.com/id/Print-Conductive-Circuits-With-An-Inkjet-Printer/.

APPENDIX A: Modified Printers

The secondary aim of the thesis is to modify two printers which are to be used in the further steps of the project. Modification is conducted to enable printers to print silver and protein ink.

Silver Ink Printing

The aim of using a modified printer instead of screen printing method is to decrease the time required for fabrication process. Brother MFC-J200 is chosen as the printer to print silver ink whose data sheet is given in the appendix. Our choice is based on the research which shows that this printer can release higher amounts of ink at a time. Higher amounts of ink provides more conductive line and hence, enables to print completely conductive pad in lesser times of repetition [76] [77].
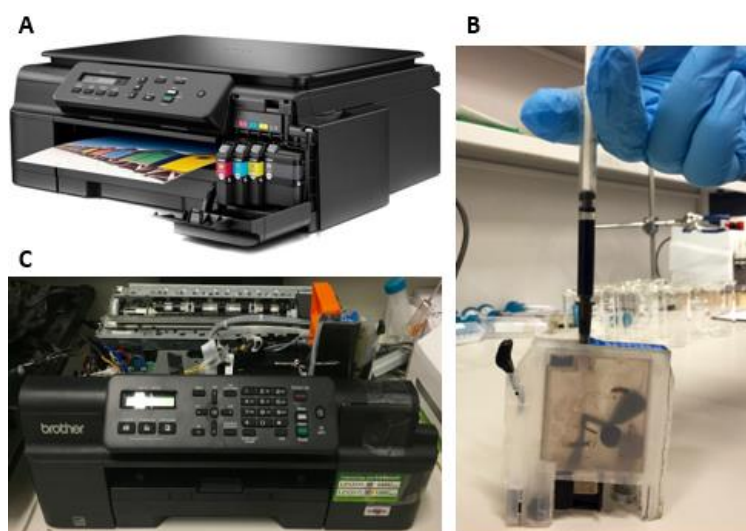

Figure 0.1. Brother MFC-J200 (A)Original printer (B) Addition of silver nanoparticle ink to the fillable cartridge (C) Printer without the covers

In the modification process, the first step is to remove the scanner and the coverage of the printer as seen in Figure 0.1. Then, the printer's original cartridges are changed with the fillable ones and the black colored cartridge is filled with the silver nanoparticle ink (Mitsubishi Paper Mill – part no: NBSU MU01).

After the modification process, the technical drawings for calibration test, which are shown in Figure 0.2 (A), are printed to learn the calibration of the printer. The calibration test results, which are shown in Figure 0.2 (B), indicate that the printer's margin of error is too high. Therefore, the printer prints the structure in larger size, multiplying the required size with the margin of error. Despite this high margin of error, the printer can still be used since weight sensors are not affected by the dimensions of the silver contact pad. As long as the pad is conductive, the dimensions of it do not matter. Therefore, there is no concern on improving the calibration test results of the printer.
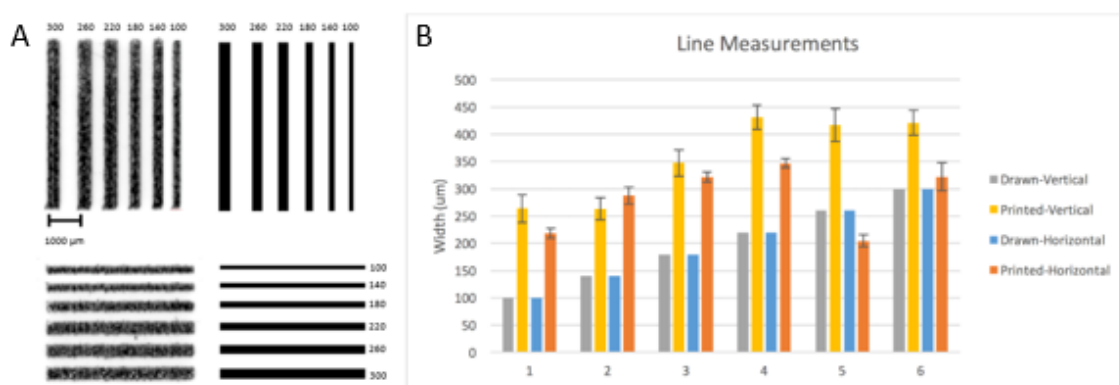

Figure 0.2. Calibration Test (A)Silver ink printed conductive line and black ink printed nonconductive line (B)Calibration test results

Protein Ink Printing

Epson L110 is chosen as the printer to print protein, Albumin. The printer for silver ink and protein ink must be different because the Brother Printer, which is the one used to print silver, operates with a fillable cartridge which is not appropriate for protein printing. It is mainly because enough amount of protein ink, considering the amount wasted by the cartridge itself, cannot be produced. Therefore, in protein printing, a printer without cartridge apparatus must be used and Epson is one of them.

In the modification process, firstly, the plastic cover of printer, the rails and the pipes are removed as seen in Figure 0.3. Then, the printer is cleaned to get rid of dust and inks and the cartridge is replaced with pipette tips. Those are then filled with the protein ink.
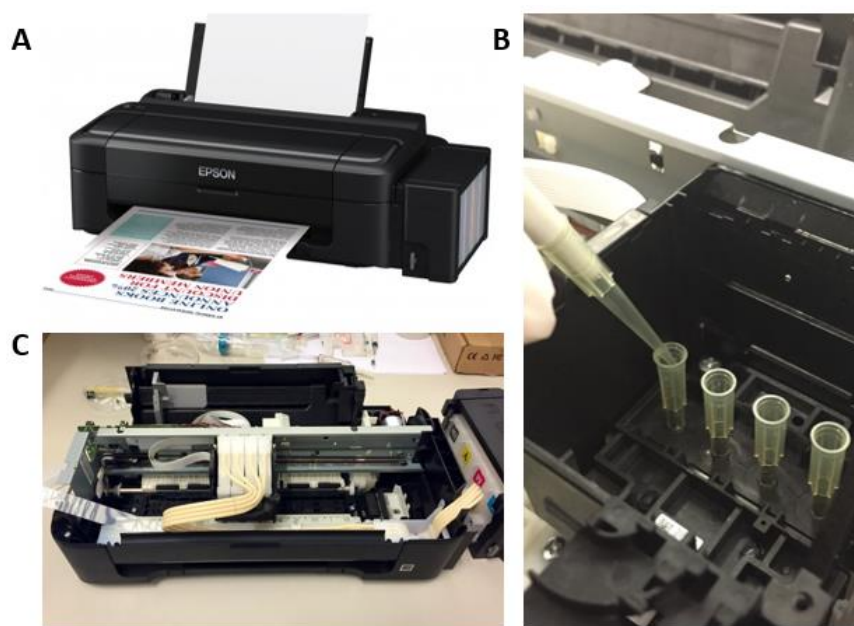
Figure 0.3. Epson L110 (A)Original printer (B)Addition of protein ink to the cartridge entrance (C) Printer without the covers

Protein ink is a combination of albumin protein, triton and double distilled water. Albumin protein is chosen because it is easily accessible protein and its binding willingness is high. Triton has an opposite impact since it decreases the binding willingness of albumin protein. High willingness is desirable because the protein should be bound to paper; yet, triton is also essential because the protein should not be bound to printer's apparatuses. Double distilled water is added to arrange the solution concentration since a level of liquidity is required to enable printer to print. Regarding these factors, based on our trials, for 1mL protein ink preparation, 0.5ml of 1mg/mL BSA, 0.05mL of 0.05% Triton X-100 and 0.45 mL of Double Distilled Water are mixed.

The calibration test is conducted also for protein printing. In Figure 0.4, the technical drawings used for the test and the results are shown.
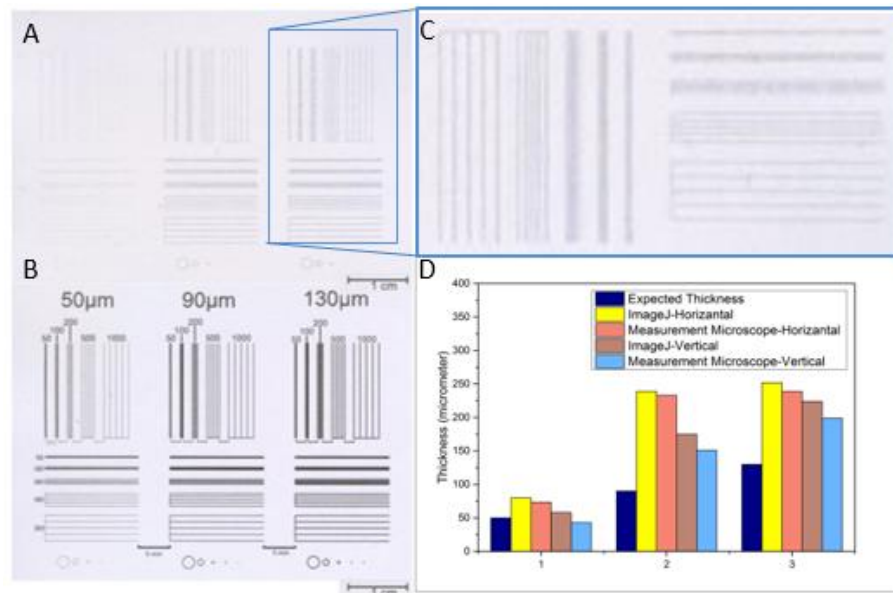

Figure 0.4. Calibration test for protein ink printing. (A) Vertically and horizontally protein ink printing. (B) Vertically and horizontally black ink printing. (C) Rotated (90 degree) and zoomed printed protein lines. (D) Calibration test results for both measurement microscope and ImageJ
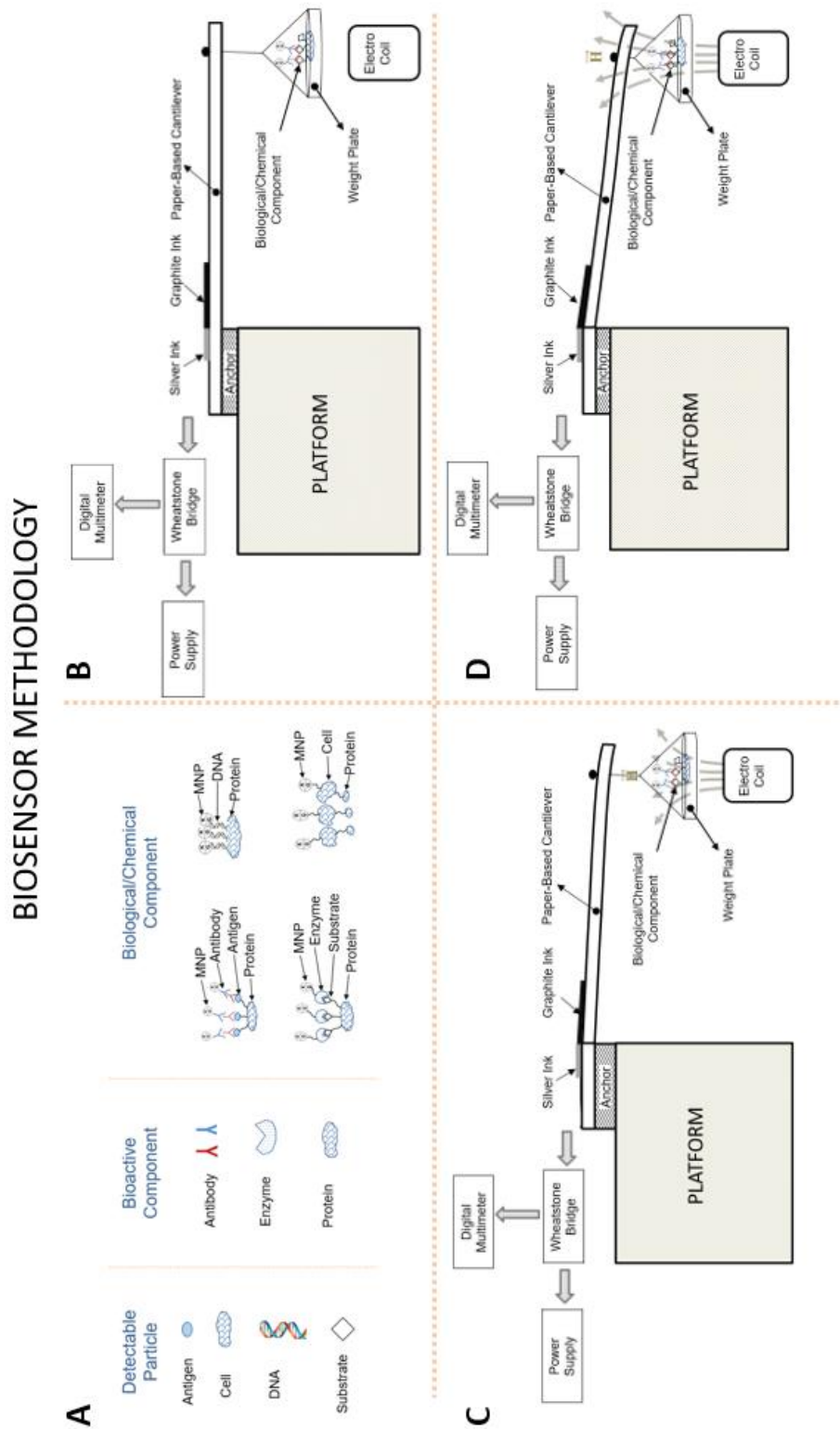
APPENDIX B: METHODOLOGY OF PIEZORESISTIVE BIOSENSOR

Figure 0.1. (A) Types of Biological/Chemical Components (B)Initial condition of the Biosensor (C)Electro Coil is activated (D) The Force of the electro coil is at maximum value

APPENDIX C: DATA SHEETS

PRODUCT SPECIFICATIONS

TECHNOLOGY

Printing Method	On-demand inkjet (Piezo electric)
Minimum Droplet Size	3 pl, With Variable-Sized Droplet Technology
Ink Technology	Epson Dye Ink
Printing Resolution	5,760 x 1,440 dpi

PRINT

Printing Speed ISO/IEC 24734 6 Pages/min Monochrome, 3 Pages/min Color

Draft printing speed	27 Pages/min Monochrome (plain paper 75 g/m²), 15 Pages/min Color (plain paper 75 g/m²), 69 Seconds per 10 x 15 cm photo (Epson Premium Glossy Photo Paper)
Colours	Black, Cyan, Yellow, Magenta

For detailed information on printing speeds please visit http://www.epson.eu/testing.

PAPER / MEDIA HANDLING

Number of paper trays	1
Paper Formats	A4, A5, A6, B5, C6 (Envelope), DL (Envelope), No. 10 (Envelope), Letter, 10 x 15 cm, 13 x 18 cm, User defined, Legal
Duplex	Manual
Paper Tray Capacity	50 Sheets Standard, 50 Sheets maximum, 10 Photo Sheets

GENERAL

Energy Use	ENERGY STAR® qualified all-in-one, 1.2 W (sleep mode), 10 W (printing)
Product dimensions	472 x 222 x 130 mm (Width x Depth x Height)
Product weight	2.7 kg
Noise Level	5.1 B (A) with Epson Premium Glossy Photo Paper / Photo RPM mode - 38 dB (A) with Epson Premium Glossy Photo Paper / Photo RPM mode
Compatible Operating Systems	Mac OS 10.5.8 or later, Mac OS 10.6+, Windows 7, Windows 7 x64, Windows 8 (32/64 bit), Windows Vista, Windows XP, Windows XP x64

LOGISTICS INFORMATION

SKU	C11CC60301
	C11CC60301DA
Barcode	8715946523507
Dimensions Single Carton	548 x 311 x 209 mm
Carton Weight	4.12 Kg
Country of Origin	Philippines
Pallet Size Euro	40 Units (4 x 10)

Epson L110

WHAT'S IN THE BOX

- Power cable
- Setup guide
- Software (CD)
- User manual (CD)
- 4 x 70ml individual ink bottles (Bk,C,Y,M)

INK CARTRIDGE COMPATIBILITY

- ● T6641
- ● T6642
- ● T6643
- ● T6644

INK YIELD DATA

4-colour ink bottles for L-Series T6644

●	4,000 pages*
●●●	6,500 pages*

* Approx. page yield based on ISO/IEC 24711 /24712 or ISO/ IEC 29103/29103. Actual yield will vary depending on images printed and usage conditions. For more information visit %LINK%

1. (s1) Quoted yields/CPP are extrapolated based on Epson original methodology from the print simulation of Test Patterns provided in ISO/IEC 24712. Quoted yields/CPP are NOT based on ISO/IEC24711. Quoted yields/CPP may vary depending on the images that you are printing, the paper type that you are using, the frequency of your prints and environmental conditions such as temperature
2. ² Comparison made with Epson L200 integrated ink tank system

EPSON®

MITSUBISHI PAPER MILLS LIMITED

Technical Data Sheet (Preliminary)

agnano@mpm.co.jp / www.mpm.co.jp

Mitsubishi Nano Benefit Series
NBSIJ-MU01 (Silver Nano Particle Ink)

Product: NBSIJ-MU01 is the waterborne silver nanoparticle ink for inkjet printing.

Benefits: Optimized for Mitsubishi Nano Benefit Series Special Media.

Suitable for major inkjet heads.

Physical properties	Result	Unit	Standard
Silver concentration	15	wt%	-
Viscosity	2.30 ± 0.50	mPa·s	JIS K 7117-2 at 25°C
Surface Tension	32.0 ± 2.0	mN/m	Wilhelmy plate method
Density	1.200 ± 0.020	g/mL	JIS B 7525
Pattern Conductivity	0.1-0.2	Ohm/sq.	apply 20-30mL/m^2 for our media
Stability	6	month	store at 0-8 degC

Inkjet Printing on Mitsubishi Nano Benefit Series Special Media

· Please filter the ink with proper syringe filters (5.0 microns pore size recommended) prior to use for better jetting performance.

· Conductivity of patterns depends on humidity of printing environment. 20 degC and >40%RH is recommended. If color of patterns does not change from silver into gold-like color after printing, printing environment may be too dry.

· If color of patterns is dark metallic like below, this is the sign of ink overflowing and the conductivity of pattern may become poor.

Ink Storage Information

· Please store the ink in a refrigerator (0 to 8 degC). Excessive exposure to light and high temperature environment (>50 degC) should be avoided. Shaking is recommended prior to use.

The above mentioned data represents recommended value. Changes in the product design due to technical further developments will not be announced in advance.

Version: Jun. 2012

MFC-J200 InkBenefit Technical Specifications

Brother's MFC-J200 InkBenefit is designed for reliability, consistent quality and cost-savings to meet the demands of a high print volume business.

Now, with affordable InkBenefit cartridges that boast 2,400* page-yield, you enjoy both lower running costs and quality prints. In addition, Brother's Laminated Piezo Print Head minimises print head damage and enhances the durability of the machine, allowing users to save on repairs.

The MFC-J200 InkBenefit also offers N-in1 printing to save paper, and an individual ink system that allows you to only replace each colour as it runs out, reducing waste and saving you money.

Furthermore, fax capability, Wireless LAN, Mobile Print and Automatic Document Feeder capabilities help boost productivity and simplify the way you work.

Last but not least, MFC-J200 InkBenefit complies with the Energy Star standard to ensure low energy consumption.

FUNCTIONS

Print, Scan, Copy, Fax, Wireless Network, Mobile Print, Automatic Document Feeder	

GENERAL

Memory	64MB
Display	1-Line
Interface	Hi-Speed USB 2.0
Wireless Network	Yes

COLOUR PRINTER

Print Speed (Laser Comparable)	Up to 11ppm (mono) and 6ppm (colour)^
Print Speed (Fast Mode)	Up to 27ppm (mono) and 10ppm (colour)
Print Resolution	Up to 1,200 x 6,000 dpi
Borderless Printing	Yes: A4, LTR, A6, Photo(102x152mm/4"x6"), Indexcard(127x203mm/5"x8"), Photo-2L(127x178mm/5"x7")
Ink Save Mode	Yes
Mobile Print	Brother iPrint&Scan, AirPrint, Google Cloud Print™

COLOUR COPY FUNCTION

Copy Speed (Laser Comparable)^^	Up to 4.8cpm (mono) and 3cpm (colour)
Copy Resolution	Print: Max. 1200x2400 dpi Scan: Max. 1200x1200 dpi
N in 1 Copy	Yes (including ID Card Copy)
Base Colour Removal	Yes

COLOUR SCAN FUNCTION

Scan Resolution	Optical: Up to 1,200 x 2,400 dpi Interpolated: Up to 19,200 x 19,200 dpi (For XP/Vista/Windows 7/Windows 8)
"Scan To" Feature	Image, Optical Character Recognition, Email, File

COLOR FAX FUNCTION

Modem	14.4 Kbps
Memory Transmission***	Up to 170 pages
Speed Dials	40
Group Dials	Up to 6 groups
Out of Paper Reception***	Up to 170 pages
PC-Fax	Sending & Receiving# (USB only)

ADDITIONAL FEATURES

Poster Print / Copy	Yes
Enlargement / Reduction Ratio	25% - 400% in 1% increments

PAPER HANDLING

Paper Input (Standard Tray)	Up to 100 sheets
Paper Output	Up to 50 sheets
Automatic Document Feeder	Up to 20 sheets
Paper Handling Sizes (Standard Tray)	A4, LTR, EXE, A5, A6, Photo (102x152mm / 4"x6"), Indexcard (127x203mm / 5"x8"), Photo-2L (127x178mm / 5"x7"), C5 Envelope, Com-10, DL Envelope, Monarch
Media Type	Plain, Inkjet, Glossy, Transparency

SUPPORTED OS AND SOFTWARE

Supported Operating Systems	Windows: XP / XP x64 / Vista / 7 / 8 Server 2003 / Server 2003 R2 / Server 2008 / Server 2008 R2 / Server 2012. Mac: OS X v10.6.8/v10.7.x/v10.8.x
Network Management Tools	BRAdmin Professional 3+, Driver DeploymentWizard+, BRAdmin Light++

SUPPLIES

Innobella™ Ink Cartridges	Super High Yield (Black) LC539XL BK: Approximate Yield 2400 A4 pages**. Super High Yield (Colour) LC535XL C/M/Y: Approximate Yield 1300 A4 pages**

DIMENSIONS & WEIGHT

Without Carton	435mm (W) x 374mm (D) x 180mm (H), 8.3kg

* Refers to black ink. Colour ink: 1,300 page-yield. Declared in accordance with ISO/IEC24711.

^ Based on ISO/IEC 24734. For more information, please refer to www.brother.com/rd/printspeed

^^ Based on ISO/IEC 24735 for the Automatic Document Feeder models. For more information, please refer to www.brother.com/rd/printspeed

+ Not supported on Mac and Linux. Available for download at http://solutions.brother.com

++ Not supported on Linux. Available for download at http://solutions.brother.com

Receiving is for Windows® only

** Approximate cartridge yield is declared in accordance with ISO/IEC 24711

*** Based on ITU-T Test Chart No 1/MMR

Brother Earth
Working with you for a better environment
www.brotherearth.com

Japanese Excellence
For Over 100 Years

143410 Conceptcc 04/14